International Journal of Nanomedicine Dovepress

Open Access Full Text Article ORIGINAL RESEARCH

A Novel Triptolide Nano-Liposome with Mitochondrial Targeting for Treatment of Hepatocellular Carcinoma

Lili Zhou[1], Yang Du[2], Yating Shang[1], Debiao Xiang[3,*], Xinhua Xia[1,*]

[1]School of Pharmacy, Hunan University of Chinese Medicine, Changsha, 410208, People's Republic of China; [2]The Second Affiliated Hospital of Hunan University of Chinese Medicine, Changsha, 410208, People's Republic of China; [3]Department of Pharmacy, The Third Hospital of Changsha, Changsha, 410208, People's Republic of China

*These authors contributed equally to this work

Correspondence: Xinhua Xia; Debiao Xiang, Email xiaxinhua001@hnucm.edu.cn; debiao-xiang@cssdsyy.com

Background: Modern pharmacological studies have demonstrated that although triptolide (TP) is effective against hepatocellular carcinoma, it has poor water solubility and more toxic side effects. In this study, we used triptolide (TP), a bioactive constituent in *Tripterygium wilfordii* Hook F, as a model drug to develop a novel nano-liposome drug delivery system for the treatment of liver tumours.

Methods: We constructed a functionally-modified triptolide liposome (FA+TPP-TP-Lips) using the film-dispersion method and investigated its physicochemical properties, mitochondrial targeting of hepatic tumour cells, in vitro and in vivo anti-hepatic tumour activity and its mechanism.

Results: The prepared FA+TPP-TP-Lips had a particle size of 99.28 ± 5.7 nm, a PDI of 0.20 ± 0.02, a zeta potential of 1.2 ± 0.08 mV, and an encapsulation rate of 74.37% ± 1.07%.FA+TPP-TP-Lips facilitates the cellular uptake of drug delivery systems and improves their targeted delivery to mitochondria. The results of cell efficacy showed that FA+TPP-TP-Lips significantly inhibited the growth of liver cancer cells, decreased mitochondrial membrane potential, and increased intracellular ROS, thus enhancing the highest apoptosis rate of liver cancer cells. The targeted liposomes (FA-TP-Lips, TPP-TP-Lips, and FA+TPP-TP-Lips) had some degree of inhibitory migration effect on Huh-7 cells relative to the unmodified TP-Lips. Studies on tumor-bearing mice demonstrated that FA+ TPP-TP-Lips effectively accumulated in tumor tissues and significantly inhibited the growth of subcutaneous tumors, achieving a tumor inhibition rate of 79.37%. FA+ TPP-TP-Lips demonstrated an enhanced anti-liver tumor effect and significantly mitigated the hepatotoxicity and systemic toxicity associated with TP.

Conclusion: In summary, the results of this study can provide a feasible solution for improving the mitochondrial targeting of nano-liposomes, and lay a foundation for further developing a novel nano targeting preparation of triptolide for the treatment of hepatocellular carcinoma.

Keywords: Triptolide, Mitochondrial Targeting, Hepatocellular Carcinoma, Folic acid, Triphenylphosphine ion

Introduction

Cancer is the second leading cause of death globally, and the Global Cancer Report 2020 indicates that by 2020, there will be 19.29 million new cancer cases and 9.96 million cancer-related deaths globally.[1–3] Global mortality and morbidity rates are increasing every year, seriously endangering the lives and health of human beings and posing a significant threat to human society.[4,5] Liver cancer is one of the leading causes of death, and it is ranked among the top 10 types of cancer in terms of global incidence and mortality.[6–8] The primary surgical interventions for patients with early to mid-stage liver cancer, including liver resection and transplantation, can yield the anticipated outcomes. However, these procedures are associated with significant drawbacks, such as elevated risk, high recurrence rates, and potential for metastasis. Furthermore, due to the difficulty in detecting early-stage liver cancer and precancerous lesions, these conditions often

Received: 26 September 2024
Accepted: 26 November 2024
Published: 3 December 2024

progress to advanced stages by the time symptoms become apparent, rendering them unsuitable for surgical intervention. Palliative treatment modalities for patients with advanced liver cancer encompass local ablation, hepatic arterial chemoembolization, radiation therapy, and pharmacotherapy. However, these interventions often induce irreversible physiological damage, thereby diminishing patient compliance and tolerance.[9,10] Consequently, the five-year relative survival rate for liver cancer remains markedly low, at merely 18%.[11] Targeted therapy has recently become a hotspot for liver cancer treatment.[12,13] It uses carriers to selectively enrich drugs in target organs, cells, or even organelles, thereby mitigating toxic side effects, reducing drug dosage, improving the safety and effectiveness of drug administration, and increasing patient compliance, which has a good application prospect.[14,15]

Triptolide (TP) is an epoxy diterpene lactone obtained from the traditional Chinese medicine *Tripterygium wilfordii* Hook.[16,17] Its molecular formula is $C_{20}H_{24}O_6$. Pharmacological studies have demonstrated that TP is a multifunctional and highly active natural product with anticancer,[18] antiinflammatory,[19,20] and immunosuppressive properties.[21] It exhibits broad-spectrum antitumour activity and can be used to treat numerous cancers, including liver,[22] lung,[23] pancreatic,[24] and breast cancers,[25] as well as rheumatoid arthritis,[26] systemic lupus erythematosus,[27] and other diseases.[28] However, the disadvantages of triptolide, including its high toxicity, narrow therapeutic window, poor water solubility, and low bioavailability, have significantly limited its clinical application.[29,30] Research indicates that TP administration is associated with the induction of toxicity across multiple organ systems, encompassing hepatotoxicity, nephrotoxicity, reproductive toxicity, cardiotoxicity, and immunotoxicity.[31,32] Through comprehensive investigation into the pharmacodynamic and toxicity mechanisms of TP, strategies to mitigate its toxicity are being identified. These strategies include employing drug delivery systems as a research approach to reduce TP's adverse effects. By selecting suitable carriers, the drug can achieve enhanced permeability and retention effects within solid tumors facilitated by macromolecular structures. This approach addresses issues related to the drug's selectivity, stability, and water solubility, modifies its pharmacokinetics, and consequently enhances the therapeutic efficacy and reduces the toxicity of TP.[33] Although liposomes have become a research hotspot for drug delivery in recent years due to their advantages, including specific targeting, slow release, and the ability to improve drug stability and bioavailability, traditional liposomes still have limitations, such as insufficiently precise targeting, poor active targeting, and insufficient in vivo circulation time.[34] These limitations can be overcome to a certain extent by functional modification of the liposome surface, which can not only enhance its targeting ability, reduce drug toxicity, but also improves drug stability and encapsulation rate.[35,36]

Folate receptors (FRs) are common tumour-targeting receptors that are overexpressed on the surface of numerous tumours, especially malignant tumours, such as breast, lung, and liver cancers.[37,38] Their expression levels increase further in advanced tumours, but are low in normal tissues and organs.[39,40] There are four subtypes of FRs: FR-α, FR-β, FR-γ, and FR-δ. Among them, FR-α and FR-β are highly expressed on the surface of tumour cells and are widely used in the targeted diagnosis and treatment of tumours.[41] Modification of folic acid on nanocarriers can further reduce its toxicity to normal cells, and give it ability to target tumour cells with high folate receptor expression.[42] Mitochondria are the biosynthetic centre of cells, which not only provide most of the energy for normal physiological activities of cells, but also participate in numerous processes such as oxidative stress, immune response, calcium ion homeostasis and the production of haematopoietic stem cells, and can also mediate cell apoptosis.[43] Therefore, mitochondrial gene mutations and other dysfunctions are closely associated with tumour generation, proliferation, survival, and metastasis.[44] Mitochondrial targeting is a common therapeutic strategy based on the important role of mitochondria in cellular metabolism and its unique structure and function.[45] It can deliver drugs directly into the mitochondria of tumour cells and is of great significance in the treatment of hepatocellular carcinoma and many other diseases. Taking advantage of the fact that the mitochondrial membrane potential is higher than that of normal cells, drug delivery to mitochondria through mitochondrial targeting groups, such as triphenylphosphine ion (TPP), Szeto-Schiller peptide, and mitochondrial penetrating peptide (MPP), is a commonly used mitochondrial targeting strategy.[46] TPP is the most widely used mitochondria-targeting moiety because of its simple structure, low cost, ease of obtaining, good biocompatibility, and rapid enrichment in tumour cell mitochondria, which can reduce or avoid damage to normal cells.[47,48]

Based on the above theory, a functionally-modified triptolide liposome (FA+TPP-TP-Lips) was constructed in this study. FA-PEG_{3400}-DSPE modified on liposomes can specifically recognize and bind to FR on the surface of liver tumour cell membrane to achieving active targeting of liposomes, thereby improving the selectivity of TP, reducing the

aggregation of TP in normal tissues and organs, and reducing side effects. At the same time, the surface coating of liposomes with DSPE-PEG_{3400} can avoid the mononuclear phagocytosis system and ensure the long-term blood circulation of FA+TPP-TP-Lips. After the intracellular delivery of FA+TPP-TP-Lips, DSPE-TK-PEG_{2000}-TPP can target mitochondria and allow the FA+TPP-TP-Lips to accumulate around the mitochondria of tumour cells.In the microenvironment of tumour cell mitochondria with high reactive oxygen species (ROS) level, the thioketone bond (TK) in DSPE-TK-PEG_{2000}-TPP was broken, and the liposomes were endocytosed into mitochondria via uptake to complete the intramitochondrial delivery of triptolide (Scheme 1). The FA+TPP-TP-Lips developed in this study has the function of targeting liver tumour mitochondria, which can improve the aggregation of drugs in tumour tissues and organelles, achieve the purpose of increasing efficacy and reducing toxicity, and provide a feasible solution for the treatment of hepatocellular carcinoma with triptolide.

Materials

Materials

The TP raw material was acquired from Chengdu Desite Biotechnology Co., Ltd.(Chengdu, China).TP control was procured from the National Institutes of Food and Drug Control(China). Soy lecithin and FA-PEG_{3400}-DSPE were acquired from Shanghai Yuanye Biotechnology Co., Ltd(Shanghai, China). TPP-PEG_{2000}-TK-DSPE was purchased from Xi'an Rui Xi Biotechnology Co., Ltd(Xian, China). Cholesterol from Sinopharm Chemical Reagent Co., Ltd(Beijing,

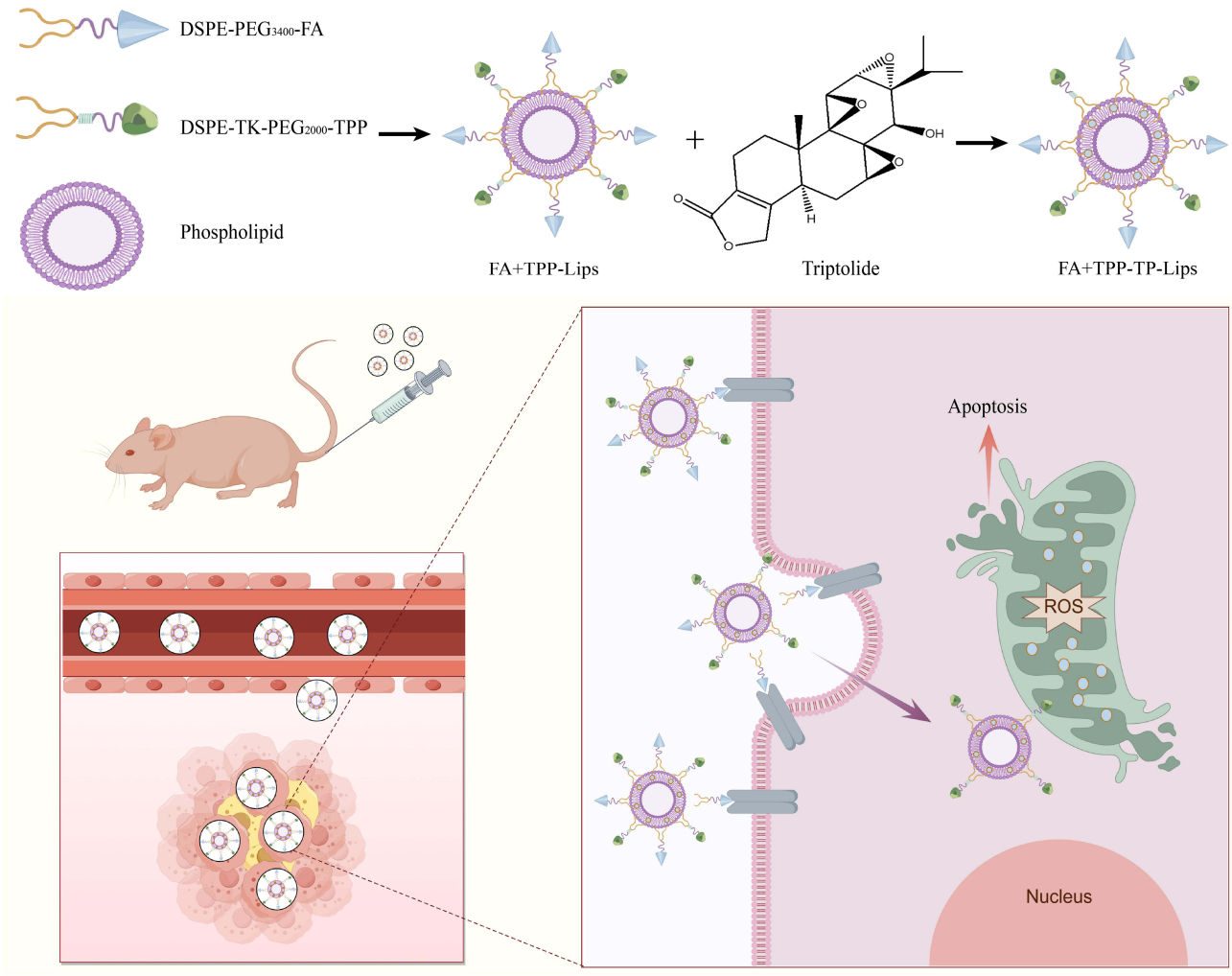

Scheme 1 Synthesis of FA+TPP-TP-Lips and its anti-hepatic tumour effects.

China). Rabbit plasma was procured from Guangzhou Hongquan Biotechnology Co., LTD(Guangzhou, China).Cy5.5 and sorafenib were obtained from MedChemExpress(Shanghai, China). JC-1 assay kit, reactive oxygen demonstration kit, Annexin V-FITC apoptosis detection kit, and Mito-Tracker Red CMXRos were procured from Becton Bio-Technology (USA). PI/RNase Staining Buffer Solution was acquired from Becton Dickinson.Co., Ltd(USA). Alanine aminotransferase (ALT), aspartate (AST), blood urea nitrogen (BUN), and creatinine (CREA) assay kits, PBS buffer (pH 7.2–7.4), penicillin-streptomycin solution, 0.25% trypsin, DMEM high sugar basal medium, and 4% paraformaldehyde were procured from Wuhan Pricella Biotechnology Co., Ltd(Wuhan, China). The primary antibody (PCNA) was obtained from the Doctoral Bioengineering Co., Ltd(Wuhan, China). fluorescent secondary antibody (CY3 goat anti-mouse) was acquired from Jackson(USA). TUNEL apoptosis detection kit and PCNA cell Proliferation detection kit were obtained from Roche(Switzerland).

Cells

Huh-7 and AML12 cells were obtained from Procell Life Science & Technology (Wuhan, China). The cells were cultured in a matching medium and incubated at 37 °C with 5% CO_2.

Animals

BALB/C nude mice (male and female, 4–5 weeks old) were acquired from Hunan Slake Jinda Laboratory Animal Co., Ltd. and housed under SPF conditions at the Laboratory Animal Management Centre of Hunan University of Traditional Chinese Medicine, with free access to food and water and acclimatisation feeding for three days before the experiments. All animal experiments adhered to ethical standards and were approved by the Experimental Animal Ethics Committee of Hunan University of Chinese Medicine (HNUCM21-2312-22).

Methods

Preparation of Triptolide Liposomes with Different Modifications

Liposomes were prepared using the film-dispersion method. Appropriate amounts of soy lecithin, cholesterol, TP, DSPE-TK-PEG_{2000}-TPP, and FA-PEG_{3400}-DSPE were weighed and placed in a pear-shaped bottle. A mixture of trichloromethane and methanol (2:1) was added and sonicated to completely dissolve them. The solvent was uniformly removed using rotary evaporation at 55 °C to form a lipid film, the film was hydrated by adding phosphate-buffered saline (PBS) (pH 6.4) for 1 h, and was sonicated with a probe for 15 min (sonication for 2 s, stop for 2 s). The liposome solution was filtered using a 0.22 μm microporous filter membrane to obtain FA+TPP-TP-Lips(TP:0.4mg/mL). The aforementioned method was used to prepare FA-TP-Lips, TPP -TP-Lips, and TP-Lips for the control test.

Characterisation of Liposomes

The evaluation indexes used to characterise the physicochemical properties of the four liposomes(FA+TPP-TP-Lips, TPP-TP-Lips, FA-TP-Lips, and TP-Lips) included morphology, particle size, zeta potential (ZP), polydispersity index (PDI), and encapsulation efficiency (EE). The microscopic morphology of the liposomes was observed using transmission electron microscopy (HITACHI, HT7800), and the particle size, ZP, and PDI were measured using a laser particle size analyser (Malvern). The encapsulation rate was determined using ultrafiltration centrifugation. Approximately 0.5 mL of liposome solution was transferred to an ultrafiltration centrifuge tube and centrifuged at 15000 r/min for 10 min. The solution outside the centrifuge tube was absorbed into the volumetric bottle, diluted up to 5mL with methanol, mixed well, filtered, and determined by high-performance liquid chromatography (HPLC) to obtain the content of free TP in the solution(M_{free}). An equal amount of liposome solution was aspirated and adjusted to 5 mL with methanol, filtered, and measured by HPLC (Agilent 1260) to obtain the total content of TP in the solution (M_{total}). The parameters for high-performance liquid chromatography were as follows: A Thermo C18 chromatographic column (150 mm × 4.6 mm, 5 μm) was utilized. The column temperature was maintained at 30°C. The mobile phase consisted of a methanol-water mixture in a 45:55 ratio. The flow rate was set at 1 mL/min, with a detection wavelength of 218 nm. The injection volume was 10 μL.The encapsulation rate was calculated by the following formula:

$$EE(\%)=(M_{total}-M_{free})/M_{total}$$

where M_{free} is the mass of free TP in liposome solution, and M_{total} is the mass of TP in liposome solution.

Haemocompatibility of Liposomes

Preparation of 2% Rabbit Erythrocyte Suspension

Approximately 50 mL of blood was collected from the rabbit heart, transferred to a conical flask containing approximately 50 glass beads, and shaken gently for 10 min to remove fibrinogen. The defibrinated blood was transferred into test tubes(5mL/tube), diluted with 30 mL of saline, mixed well, and centrifuged at 3000 r/min for 10 min. The supernatant was discarded, and the above steps were repeated until the supernatant became clear and colourless. The precipitated erythrocytes were taken from the bottom, diluted into a 2% erythrocyte suspension with saline, and stored at 4 °C for future use.

Examination of Haemolysis Experiments

TP-Lips was used as a control, and the effects of TPP-TP-Lips, FA-TP-Lips, and FA+TPP-TP-Lips on erythrocyte haemolysis were observed. According to the haemolysis experimental protocol (Table 1), 40 10 mL Eppendorf (EP) tubes were divided into four groups of 10 tubes/group, numbered 1–10, out of which No. 1–7 were the test tubes. The amount of liposomes added to the test tubes was 0.1, 0.2, 0.3, 0.4, 0.5, 0.6, and 0.7 mL, respectively. Tube 8 was used as the negative control, tube 9 as the positive control, and tube 10 as the test control. The specific amount added is listed in Table 1. The EP tubes were incubated in a thermostatic incubator (37 ± 0.5 °C) for 3 h, and the haemolysis reaction was terminated using an ice bath. The tubes were centrifuged at a low temperature for 10 min (4 °C, 6000 r/min), the colour of the supernatant and the remaining red blood cells at the bottom were used as indicators to observe the haemolytic reaction, and photos were taken. The supernatant was collected, and the 10th tube of each group was used as the reference solution to determine the absorbance at 576 nm using a UV spectrophotometer. The haemolysis rate of each group was calculated by the following formula:

$$\text{Haemolysis rate}(\%)=(Ab_{sample}-Ab_{negative})/(Ab_{positive}-Ab_{negative})\times 100\%$$

where Ab_{sample} represents the absorbance value of the sample, $Ab_{negative}$ is the absorbance value of the negative control, and $Ab_{positive}$ represents the absorbance value of the positive control.

Cell Proliferation Inhibition Assay

The CCK8 method was used to determine the effects of FA+TPP-TP-Lips on the proliferation of human hepatocellular carcinoma cells and mouse-derived normal hepatocyte AML12 cells. Huh-7 cells in the logarithmic growth phase were inoculated into 96-well culture plates (5×10^3 cells/well) and incubated at 37 °C and 5% CO_2 for 24 h to ensure cell

Table 1 Experimental Protocols for Haemolysis

No.	Volume of Samples (ml)	Volume of Saline (ml)	Volume of 2% Red Blood Cell Suspension (ml)	Volume of Deionised Water (ml)
1	0.1	2.4	2.5	0
2	0.2	2.3	2.5	0
3	0.3	2.2	2.5	0
4	0.4	2.1	2.5	0
5	0.5	2	2.5	0
6	0.6	1.9	2.5	0
7	0.7	1.8	2.5	0
8	0	2.5	2.5	0
9	0	0	2.5	2.5
10	0.7	4.3	0	0

adhesion to the wall. Subsequently, solutions containing different concentrations of FA+TPP-TP-Lips (5, 10, 20, 40, 80, 160, 320, and 640 nmol/L) were added to the cells and incubated for different times (24, 48, 72, and 96 h) followed by addition of 10 μL of CCK8 solution to each well, the incubation was continued for 2 h after gently tapping and mixing. Based on the time of drug action and concentration gradient determined in the above experiments, the effects of TP-Lips, FA- TP-Lips, TPP-TP-Lips, FA+TPP-TP-Lips, and free TP solutions on the survival rate of Huh-7 cells and AML12 cells were determined by the same method. After FA+TPP-TP-Lips treatment for different times, the absorbance values(OD) of cells at 450 nm were measured by enzyme labelling instrument, and the cell inhibition rate (IR) was calculated according to the following formula: $IR\%=(1-OD_{test}/OD_{control}) \times 100\%$. Using untreated cells as a control and considering molar concentration and cell viability ratio as parameters, the IC_{50} value was determined utilizing GraphPad Prism 9.

Cell Migration

Parallel lines were drawn on the outer bottom surface of the 6-well plates with a spacing of 0.5 cm by a pen. Huh-7 cells were digested with trypsin to prepare cell suspension. The cells were counted and spread on the plate to ensure a similar spreading density for each group of cells, and made to overgrown into a monolayer on the second day by controlling the density. A scratch was created in the monolayer using a 10 μL gun tip, the direction of the scratch was perpendicular to the marking line. The used medium was discarded, and the cells were washed thrice with PBS to remove the floating cells. The drug groups were designed as follows: TP solution, FA+TPP-TP-Lips, FA-TP-Lips, TPP-TP-Lips, and TP-Lips. The drug was diluted to the administered concentration in serum-free medium, and the control group was supplemented with an equal amount of serum-free medium. Three compound wells were set in each group and incubated at 37 °C and 5% CO_2. Cell migration was observed under a microscope at 0, 24, 48, and 72 h. The pre-made markers were used as fixed observation points to capture pictures at regular intervals. The images were analysed using ImageJ software, and the width of the scratches at each time point was determined. Cell migration was calculated by the following formula:

$$\text{Cell migration rate} = (\text{initial width} - \text{endpoint width})/\text{initial width} \times 100\%$$

Cellular Uptake Experiments

As TP itself is non-fluorescent, in order to investigate the uptake behaviour of liposomes in Huh-7 cells, a fat-soluble fluorescent dye with green fluorescence, C6, was used as a model drug to replace TP. FA+TPP-C6-Lips, FA-C6-Lips, TPP-C6-Lips, and C6-Lips were prepared as previously described. Laser confocal microscopy(Olympus) was used to observe the uptake of C6-labelled liposomes by Huh-7 cells. Huh-7 cells in the logarithmic growth phase (1×10^5 cells/well) were inoculated in 35 mm laser confocal dishes for 24 h. C6-labelled liposome solution (1 mL) was added and incubated for 4 h. The medium was discarded, and the cells were washed thrice with PBS. A JC-1 (100 nmol/L) mitochondrial membrane potential fluorescent probe (red) diluted in serum-free medium was added and incubated for 20 min. The culture medium was aspirated, and the cells were washed twice with 0.5 mL of PBS. Approximately 0.5 mL of cell tissue fixative was added to each well and incubated for 5 min. The fixative was removed, and the cells were washed twice with 0.5 mL of PBS. Next, 50 μL of DAPI (10 μg/mL, stain the nucleus blue) was added so that the cells were completely covered and incubated for 10 min. The staining solution was removed, and the cells were washed twice with 0.5 mL of PBS. An anti-fluorescent bursting agent (10 μL) was added dropwise to each slide, and coverslips were removed from the 24-well plate and affixed to the slides. The distribution of FA+TPP-C6-Lips, FA-C6-Lips, TPP-C6-Lips, C6-Lips, and C6 solutions in tumour cells was observed by laser confocal microscopy(Olympus).

Observation of Mitochondrial Morphology

Huh-7 cells with 80% growth fusion were digested and seeded into 20 mm confocal Petri dishes, and incubated for 4 h after adding 1 mL of TP solution, TPP-TP -Lips, FA-TP-Lips, FA+TPP-TP-Lips, and TP-Lips, respectively. After the intervention, the culture solution was sucked off and the cells were washed thrice with PBS, and mixed thoroughly with 1 mL of pre-warmed Mito-Tracker Red CMXRos working solution (1 μL Mito-Tracker Red CMXRos stock solution + 1 mL of fresh MEM culture solution), and incubated at 37 °C for 20 min. The working solution was then aspirated, 2 mL

of MEM culture solution was added, and the mitochondrial morphology of the cells was observed under a laser confocal microscope (×100).

Measurement of Mitochondrial Membrane Potential

Huh-7 cells were digested and seeded into a 20 mm confocal Petri dishes for treatment. At the end of the intervention, the culture medium was removed, then the cells were washed once with PBS, mixed thoroughly with 1 mL of JC-1 staining working solution, and incubated at 37 °C for 24 h. The working solution was then aspirated, and the cells were washed twice with JC-1 staining buffer and mixed with 2 mL of MEM culture solution, and the change of mitochondrial membrane potential in the cells was observed by the laser confocal microscope.

Detection of ROS Level

Huh-7 cells in the logarithmic growth phase were selected, monolayer cells were digested using 0.25% trypsin, and a single-cell suspension was prepared with DMEM high glucose medium containing 10% calf serum. The cells were inoculated in 6-well plates at a density of 5×10^5 cells/well and incubated at 37 °C for 24 h with 5% CO_2, followed by the addition of TP solution, TP-Lips, FA-TP-Lips, TPP-TP-Lips and FA+TPP-TP-Lips, and cultured for 48 h. The single-cell suspension from each treatment group was collected by centrifugation, washed twice with PBS, and the supernatant was discarded. The cells were resuspended in DCFH-DA staining solution diluted in serum-free medium and incubated at 37 °C for 20 min in the dark with shaking and mixing every 3–5 min. The cells were then washed thrice with PBS, resuspended in serum-free cell culture medium, filtered through a 200-mesh sieve, and the filtrate was collected. The blank cells were used as the control group, the fluorescence values of cells in each treatment group were determined at the excitation wavelength of 485 nm and the emission wavelength of 525 nm by Flow cytometry(Beckman).

Apoptosis Detection

Cells in the logarithmic growth phase were taken, digested with trypsin, and resuspended in complete medium. After the cell concentration was adjusted to 1×10^5 cells/mL, the cells were inoculated into 6-well plates at a concentration of 3 mL/well, and incubated at 37 °C and 5% CO_2 for 24 h. When the fusion rate of the growing cells reached 60%, the culture medium was discarded, and the cells were washed thrice with PBS. Different media containing TP solution, TP-Lips, FA-TP-Lips, TPP-TP-Lips, FA+TPP-TP-Lips, and sorafenib were respectively added to different experimental groups, and 3 mL of basal medium was added to blank control group. After 48 h of drug administration, the cells were digested using EDTA-free trypsin, 1×10^6 cells were collected from the control and treatment groups, respectively, and centrifuged at 1000 r/min for 5 min at 4 °C. The supernatant was discarded, and 1 mL of pre-cooled PBS was added. The mixture was gently shaken to obtain a complete suspension, centrifuged at 1000 r/min for 5 min at 4 °C, and the supernatant was discarded. The cells were resuspended in 200 μL of Binding buffer, 10 μL of Annexin V-FITC and 10 μL of PI were added. The obtained mixture was gently mixed well, and incubated at 4 °C in the dark for 30 min, 300 μL of binding buffer was added, and apoptosis was analysed using flow cytometry(Beckman).

Evaluation of Tumor Tissue Targeting Ability

Fluorescent liposomes containing a small amount of Cy5.5 were prepared according to the liposome preparation method and stored. Huh-7 cells were collected and diluted in a mixture of PBS and matrix gel (1:1) to a concentration of 2×10^6 cells/mL. 0.1 mL of diluted cell solution was inoculated into the axilla of BALB/c nude mice aged 5 to 7 weeks to establish a tumour-bearing mouse model. When the transplanted tumour grew to 200 mm^3 in size, the animals were randomly divided into five groups: Lips, FA+TPP-cy5.5-Lips, FA-Cy5.5-Lips, TPP-Cy5.5-Lips, Cy5.5-Lips, (three animals in each group and a total of 15 animals), and labelled. After administration of the drugs through tail vein injection, the BALB/c nude mice were anesthetized with isoflurane at 16h and 24 h respectively, and then in vivo fluorescence imaging was performed. Finally, BALB/c nude mice were executed by cervical dislocation, and the liver, spleen, kidney, heart, and lungs were removed under aseptic conditions, and the tumours were isolated for ex vivo fluorescence imaging.

In vivo Antitumour Effect

When the transplanted tumour grew to 80 mm^3, the mice were randomly divided into eight groups (5 in each group, a total of 40 mice), and labelled. Mice in each group were administrated saline, sorafenib, FA+TPP-TP-Lips, FA-TP-Lips, TPP-TP-Lips, TP-Lips, TP-Lips, and TP solution (TP: 0.2 mg/kg) by tail vein injection on day 0, 3 and 6, respectively. During administration, the tumour size was measured every three days using Vernier callipers, and the growth curves were plotted as a reference. On the 9^{th} day after administration, blood was collected from the ocular venous plexus to measure blood routine, liver and kidney functions and other biochemical indexes. Meanwhile, tumour tissues of mice were collected, weighed and photographed. The tumor inhibition rate is calculated as follows:

$$\mathrm{IR}\% = (1 - \mathrm{OD\ of\ the\ subject\ group}/\mathrm{OD\ of\ the\ control\ group}) \times 100\%$$

Immunohistochemistry

The structures of major organs and tumor tissues were observed by hematoxylin and eosin (H&E) staining. Following the treatment, the mice were euthanized via cervical dislocation. Major organs(heart, liver, spleen, lungs, and kidneys) along with tumors, were isolated and collected, followed by fixation in 4% paraformaldehyde for a duration of 24 hours. Following the pruning of these tissues, they underwent a gradual dehydration and clearing process using a series of alcohol and xylene solutions at varying concentrations. Subsequently, the tissue is immersed in paraffin and embedded to create a complete bulk specimen, which is then affixed to the microtome. Utilize a microtome to section specimens into slices approximately 4 μm in thickness. Hematoxylin and eosin (H&E) staining was performed for a duration of 3 to 5 minutes. Following the completion of the staining process, the tissue sections undergo a series of dehydration steps and are rendered transparent through the application of xylene. Finally, the slices are hermetically sealed. These treated and stained sections were observed under an optical microscope to evaluate histopathological changes during treatment.

The apoptosis of tumor cells was evaluated by TUNEL staining. The paraffin-embedded tissue sections stored at room temperature were sequentially immersed in xylene for 3 minutes, followed by anhydrous ethanol for 5 minutes, 85% ethanol for 5 minutes, and 75% ethanol for 5 minutes, after which they were washed in deionized distilled water (ddH_2O) for 5 minutes. The tissue sections were placed in a repair box filled with EDTA antigen repair solution and the antigen repair was carried out in a microwave oven (medium fire 8 min, ceasefire 8 min, medium low fire 7 min). Following natural cooling, perform three washes using a decolorizing shaker with phosphate-buffered saline (PBS), allowing 5 minutes for each wash. Subsequently, it was sealed in 3% goat serum at room temperature for 30min. Carefully agitate the sealing solution, then combine reagent 1 (TdT) and reagent 2 (dUTP) from the TUNEL kit in a 1:10 ratio. Subsequently, arrange the slices horizontally in a humidified chamber at 4°C overnight, ensuring to add a minimal quantity of water to the chamber to sustain humidity levels. Following the drying of the slices, DAPI dye was applied to the designated area and incubated at room temperature for 10 minutes. Subsequently, the sample was treated with an anti-fluorescence agent to quench the fluorescence. Subsequently, the sections were sealed using an anti-fluorescence quenching agent. Samples were examined using an inverted fluorescence microscope, and corresponding images were acquired for analysis.

The proliferative activity of cells within tumor tissues was assessed through the application of PCNA staining. Paraffin-embedded tissue sections that had been stored at room temperature were subjected to a dewaxing process. A citric acid solution (1×, pH 6.0) was employed as the repair medium, with the repair process conducted under conditions of elevated temperature and pressure. After repair, 10% goat serum was incubated at 37°C for 30min for closure. Dry the sealing liquid, add a primary antibody, and place the slices flat in a wet box at 4 °C overnight.The slides were placed in PBS (pH 7.4) and washed 3 times on a decolorizing shaker for 5 min each time. After the sections were slightly dried, a secondary antibody working solution was added dropwise and incubated at room temperature for 1 h. The tissue samples were treated with DAPI, incubated at room temperature for 5 minutes, and subsequently washed three times with PBS, with each wash lasting 5 minutes. Subsequently, the sections were sealed using an anti-fluorescence quenching agent. The treated sections were examined by fluorescence microscope under each channel, and the proliferation index was calculated.

Safety Evaluation

During the entire experiment, the body weight of the mice was recorded every three days to calculate the rate of weight change.The weight change rates were calculated as [($weight_{after}$ -$weight_{before}$)/$weight_{before}$*100%]. H&E staining was performed on the major organs (heart, liver, spleen, lungs, and kidneys). The levels of serum AST, ALT, BUN, and CREA were measured.

Statistical Analysis

The experimental data are expressed as the mean±SD and were plotted and analyzed using GraphPad prism 9. All statistical analyses were performed using the one-way ANOVA. Significance was determined according to the following thresholds: *p<0.05, ** p <0.01, *** p <0.001, **** p <0.0001.

Results and Discussion

Characterisation of Liposomes

TP is a hydrophobic drug with poor solubility in water. Liposomes are mostly composed of phospholipids and cholesterol, which can encapsulate the insoluble drugs between lipid bilayer, and can be used to construct the nano-preparation loaded with hydrophobic drugs. Four types of liposomes loaded with TP (FA+TPP-TP-Lips, TPP -TP-Lips, FA-TP-Lips, and TP-Lips) were prepared using the film dispersion method. From the appearance observation, the formed lipid film was uniform and delicate, and the liposome solution was transparent with light blue opalescence. During tumour treatment, the particle size is the main factor affecting the cellular uptake rate and in vivo circulation time of liposomes. The particle size distribution, PDI, and ZP of the four liposomes were determined by dynamic light scattering method(Figure 1B and C, Table 2). The particle sizes of the four liposomes were small (< 150 nm) and uniformly distributed (PDI < 0.2). The ZP results revealed that the surface charge of liposomes modified with DSPE-TK-PEG_{2000}-TPP and FA-PEG_{3400}-DSPE changed from negative to positive. Because the mitochondrial membrane of tumor cells is more negatively charged than that of normal cells, the modified liposomes are more likely to be close to mitochondria, exhibiting mitochondrial targeting ability. Transmission electron microscopy revealed that the four liposomes were monodisperse and spherical(Figure 1A). Compared with TP-Lips, the liposomes modified by guiding molecules were more rounded, which might be due to the fact that the PEG long chains in the guide molecule could form a hydration layer on the surface of the liposomes, reduce the surface tension of the liposomes, and enhance their stability and integrity. Moreover, the encapsulation rate is an important parameter for evaluating the characteristics of the liposome carriers. In this study, the encapsulation rate of the TP liposomes was determined by high-speed centrifugation method. The results revealed that the encapsulation rates of all four liposomes were more than 70%. Compared with TP-Lips, the encapsulation rate of liposomes modified by the guiding molecule did not decrease significantly, indicating that the encapsulation ability of liposomes to TP was unaffected by the targeted modification groups.

Haemolysis Experiment

By examining the haemolysis of TPP-TP-Lips, FA-TP-Lips, and FA+TPP-TP-Lips at different concentrations, the haemocompatibility of liposomes was investigated to reflect the safety of liposomes for intravenous injection. After samples were added to tubes 1–7, the supernatants were colourless and transparent. The erythrocyte precipitation at the bottom was undifferent from that of the negative control tube (tube 8), and no haemolysis was observed by the naked eye (Figure 2), demonstrating that the liposomes met the biocompatibility requirements for intravenous injection within the experimental concentration range. The absorbance values of the liposomes in each group were determined using a UV spectrophotometer, and the haemolysis rate was calculated. The results revealed that the haemolysis rates of tubes 1–7 were less than 5%, the haemolysis rate of blank liposomes was less than 2%, and the haemolysis rate did not change significantly after the addition of TP, indicating that TP did not cause haemolysis after encapsulation by liposomes. The haemolysis rate of liposomes modified with guiding molecular was slightly increased, but not more than 4%, which still met the requirements for intravenous injection.

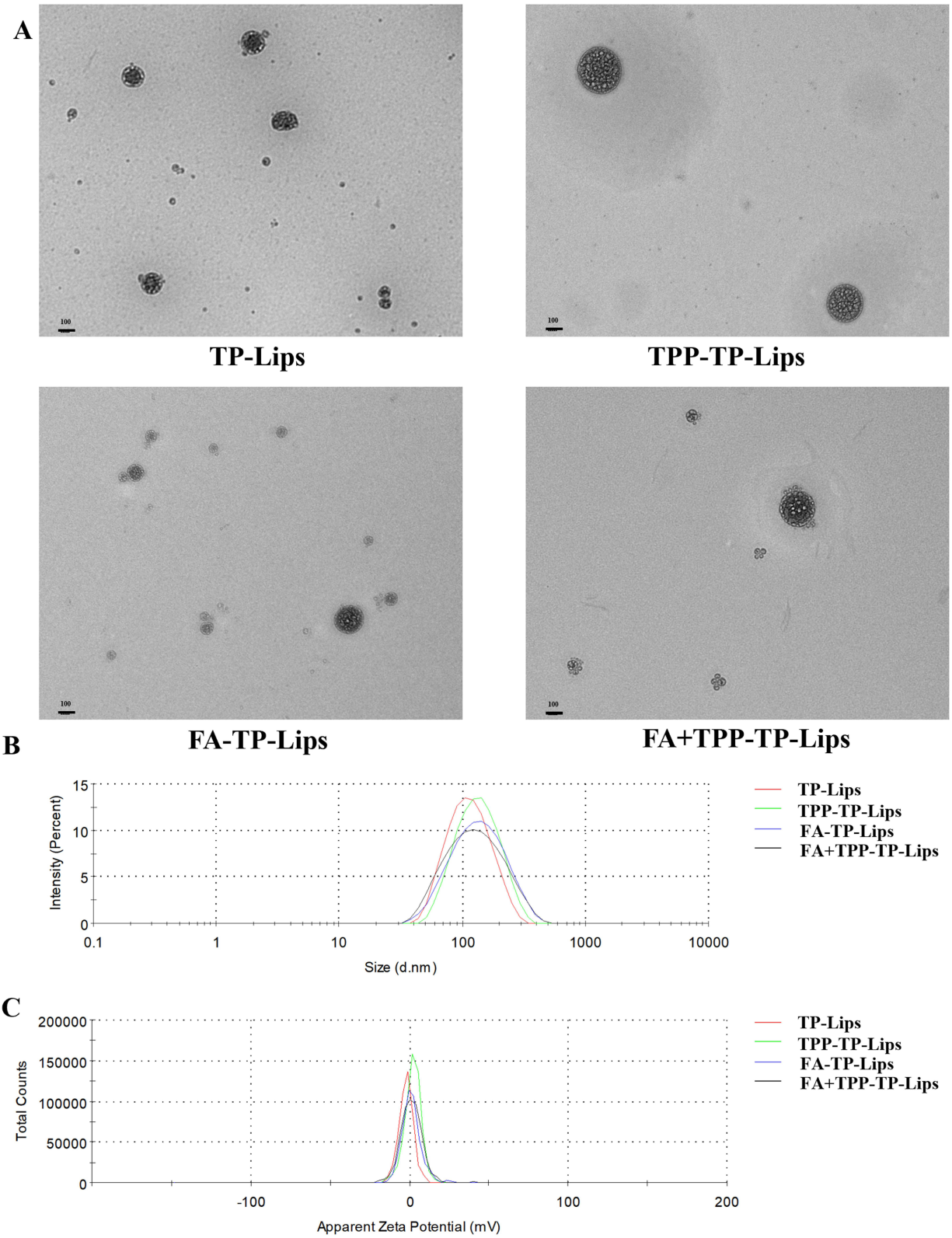

Figure 1 Characterisation of liposomes.(**A**)Transmission electron micrographs of liposomes.(**B**) Size distributions.(**C**) Zeta potential.

Table 2 Particle Size, ZP, and EE of Different Types of Liposomes

Type of Liposomes	Particle Size (nm)	PDI	Zeta Potential (mV)	EE%
TP- Lips	104.1±0.9	0.17±0.02	−2.68±0.83	72.15%±1.21
TPP -TP - Lips	96.29±1.6	0.20±0.02	2.17±0.23	72.58%±0.98
FA-TP- Lips	106.9±2.0	0.19±0.02	1.09±0.28	74.10%±1.34
FA+TPP- TP-Lips	99.28±5.7	0.20±0.02	1.2±0.08	74.37%±1.07

Cell Proliferation Inhibition Experiment

As shown in Figure 3, FA+TPP-TP-Lips inhibited the proliferation of Huh-7 cells in dose- and time-dependent manner. At the same concentration, the proliferation inhibitory effect of, FA+TPP-TP-Lips on Huh-7 cells increased with prolonged action time, and the effect on the survival rate was relatively significant. At 72 and 96 h, the inhibitory effect of the drug on the proliferation of Huh-7 cells did not change significantly with the increase of time. Therefore, the final action time of FA+TPP-TP-Lips was set at 72 h. The IC_{50} values of four liposomes and TP solution on Huh-7 and AML12 cells are depicted in Figure 3. The IC_{50} values of TP solution in Huh-7 and AML12 cells were lower than those of the TP liposome groups, and there were a significant difference, indicating that the cytotoxicity of TP solution was higher, and liposome encapsulation exhibited a better effect of "enhancing effect and reducing toxicity". There was a significant difference between FA+TPP-TP-Lips and TP-Lips, indicating that the inhibitory effect of liposomes on

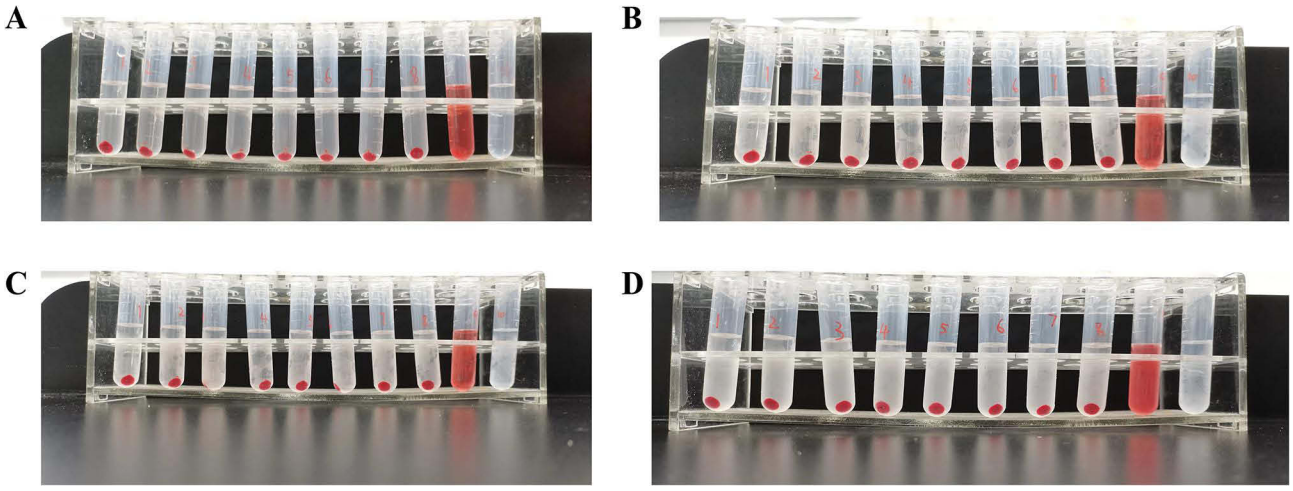

Figure 2 Haemolytic assessment of liposomes.(**A**) TP-Lips; (**B**) TPP-TP-Lips; (**C**) FA-TP-Lips; (**D**) FA+TPP-TP-Lips.

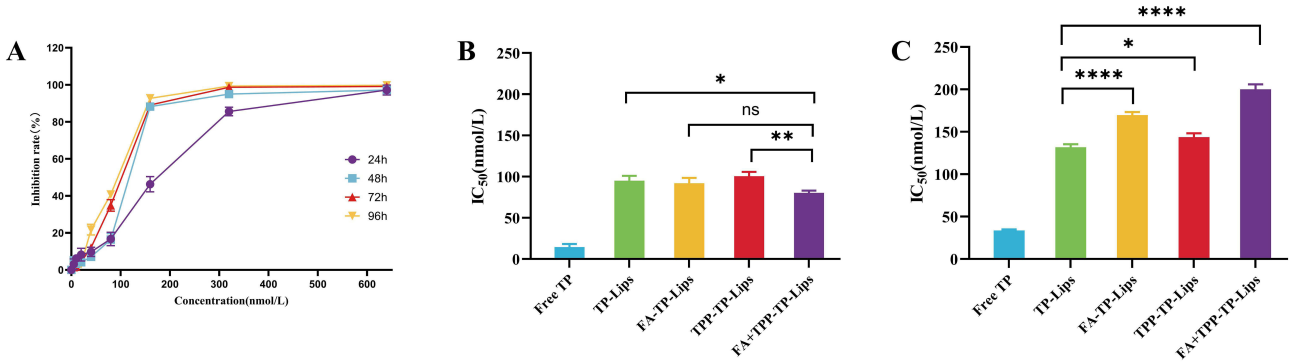

Figure 3 Inhibitory effect of liposomes on Huh-7 and AML12 cell proliferation (n = 3). (**A**) Cell inhibition rate of FA+TPP-TP-Lips at different action times. (**B**) IC_{50} values of different experimental groups acting on Huh-7 cell line. Data are expressed as the mean±SD (n=3), (**C**) IC_{50} values of different experimental groups acting on AML12 cell line. Data are expressed as the mean±SD (n=3). *$p < 0.05$, ** $p < 0.01$, **** $p < 0.0001$.

hepatocellular carcinoma cells and hepatocyte proliferation was enhanced by the guiding molecule modification, which may be attributed to the fact that Huh-7 and AML12 cells have greater uptake capacity of TP liposomes modified by guiding molecule than TP-Lips. This uptake may depend on the binding of the guiding molecules to receptors on the surface of Huh-7 and AML12 cells, improving the affinity of liposomes to hepatocellular carcinoma cells and hepatocytes. Moreover, the IC_{50} values of four liposomes in Huh-7 cells were significantly lower than those in AML12 cells, indicating that the modified TP liposomes were more toxic to tumour cells and exhibited preliminary liver tumour-targeting characteristics.

Cell Migration

The cell migration rate after treatment is illustrated in Figure 4. Compared with the TP solution group, the migration inhibition effect of various TP liposomes on Huh-7 cells was enhanced, indicating that the encapsulation of liposomes could augment the migration inhibition effect of TP on tumour cells. The targeted liposomes (FA-TP-Lips, TPP-TP-Lips,

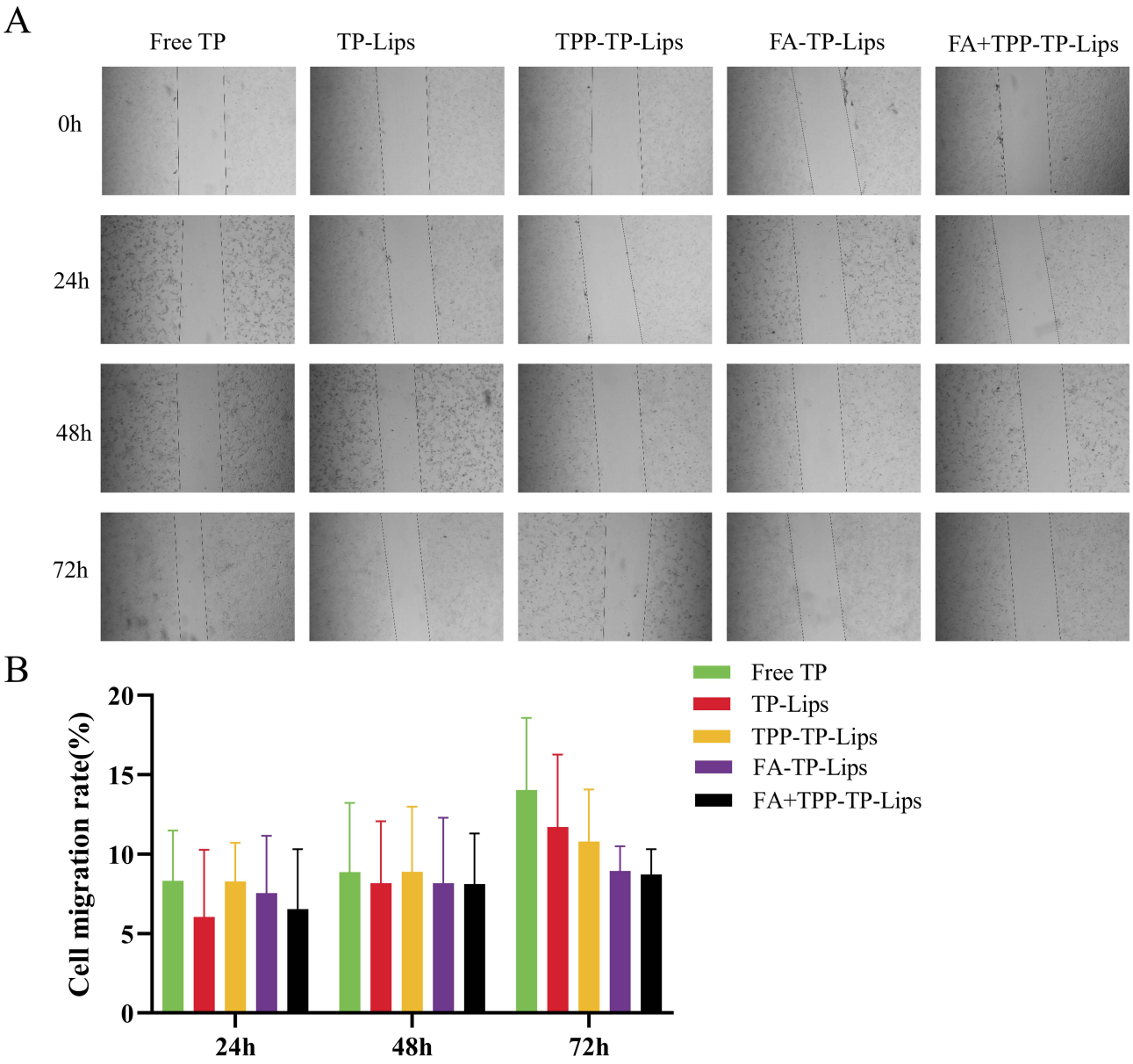

Figure 4 Effects of liposomes on Huh-7 cell migration (n = 3). (**A**) Comparative graph of Huh-7 cell migration; and (**B**) Migration rate of Huh-7 cells.

and FA+TPP-TP-Lips) had some degree of inhibitory migration effect on Huh-7 cells relative to the unmodified TP-Lips. Notably, the liposomes co-modified by FA and TPP had the most significant inhibitory effect on hepatocellular carcinoma cell migration, which may be because the combined effect of FA and TPP increased the uptake of FA+TPP-TP-Lips by cells, which is consistent with the trend of the results of the cellular uptake and CCK-8 assays.

Cellular Uptake Experiments

In this study, C6-loaded liposomes (FA+TPP-C6-Lips, FA-C6-Lips, TPP-C6-Lips, and C6-Lips) were prepared by replacing TP with C6 fluorescent dye. Huh-7 liver tumour cells were selected to evaluate cellular uptake of FA+TPP-C6-Lips, FA- C6-Lips, TPP-C6-Lips, and C6-Lips. The laser confocal microscopy images are depicted in Figure 5. In the figure, the blue fluorescence channel represents the fluorescence imaging of nuclear staining by DAPI, the red fluorescence channel represents the fluorescence imaging of mitochondrial membrane staining by JC-1, the green fluorescence channel is the fluorescence imaging of cell ingesting C6-containing nano-drug carriers, and Merge is the superimposed image of the three fluorescence channels. Green fluorescence was observed in all four C6-loaded liposome-treated cells, and the fluorescence intensity was significantly higher than that of the C6 solution, indicating that the liposomes constructed in this study were more likely to be endocytosed into cells. It is noteworthy that mitochondrial targeting (the degree of overlap between red and green) was more significant in the FA+TPP- C6- Lips group, followed by the TPP- C6-Lips group, and the mitochondrial targeting of the FA-C6-Lips group and C6-Lips group had no significant difference and was smaller than the above two groups, which may be because the mitochondrial membrane potential of the tumour cells was larger, and the cationic TPP modified liposomes were more easily enriched in the mitochondrial membrane.

Morphological Observation of Mitochondria

In order to further confirm the mitochondrial damage caused by liposomes, the mitochondria were stained with Mito-Tracker Deep Red dye, and the morphology was observed under laser confocal microscope (see Figure 6). In Huh-7 cells, the number of normal mitochondria was large, and the shape was linear and long strip, while the damaged mitochondria may exhibited the morphological changes such as vacuolisation, cristae breakage, and disappearance. The results of Mito-Tracker staining revealed that the mitochondrial damage degree of the liposome-treated cells was greater than that of TP solution, and the mitochondria in the TP solution group exhibited normal morphology, indicating that TP was more likely to be taken up and endocytosed into cells after being loaded with liposome. Further observation of the mitochondrial damage caused by the four liposomes revealed that FA+TPP-TP-Lips caused significantly more damage to the mitochondria of Huh-7 cells than TP-Lips, FA-TP-Lips and TPP -TP -Lips, and the morphology of the mitochondria changed from strip or tubular to granular and fragmented, which further verified that the liposomes co-modified by FA and TPP could not only actively target to the surface of the tumour cells faster to be taken up and endocytosed, but also precisely act on the mitochondria after entering the cells, which was consistent with the results of the cellular uptake experiments.

Mitochondrial Membrane Potential Assay

To investigate the effects of drug transport to the mitochondria on mitochondrial membrane potential, the cationic dye JC-1 was used to measure the alteration of mitochondrial membrane potential by TP solution, TP-Lips, FA-TP-Lips, TPP-TP-Lips, and FA+TPP-TP-Lips. When the mitochondrial state is normal, JC-1 accumulates in the matrix of mitochondria in the form of JC-1 aggregate and emit red fluorescence. When the mitochondrial membrane potential is reduced, JC-1 exists in the cytoplasm as a JC-1 monomer and produces green fluorescence. Therefore, the change in mitochondrial membrane potential can be measured based on the relative ratio of JC-1 aggregate/JC-1 monomer. As shown in Figure 7, the the ratio of JC-1 aggregate/JC-1 monomer in the mitochondria of blank group was higher, indicating less damage to the mitochondria. The ratio of JC-1 aggregate/JC-1 monomer in the mitochondria of TPP-TP-Lips group was lower than that of FA-TP-Lips. Notably, the ratio of JC-1 aggregate/JC-1 monomer of FA+TPP-TP-Lips was significantly lower than that of TPP-TP-Lips, FA-TP-Lips and TP-Lips, confirming that TP liposomes co-modified

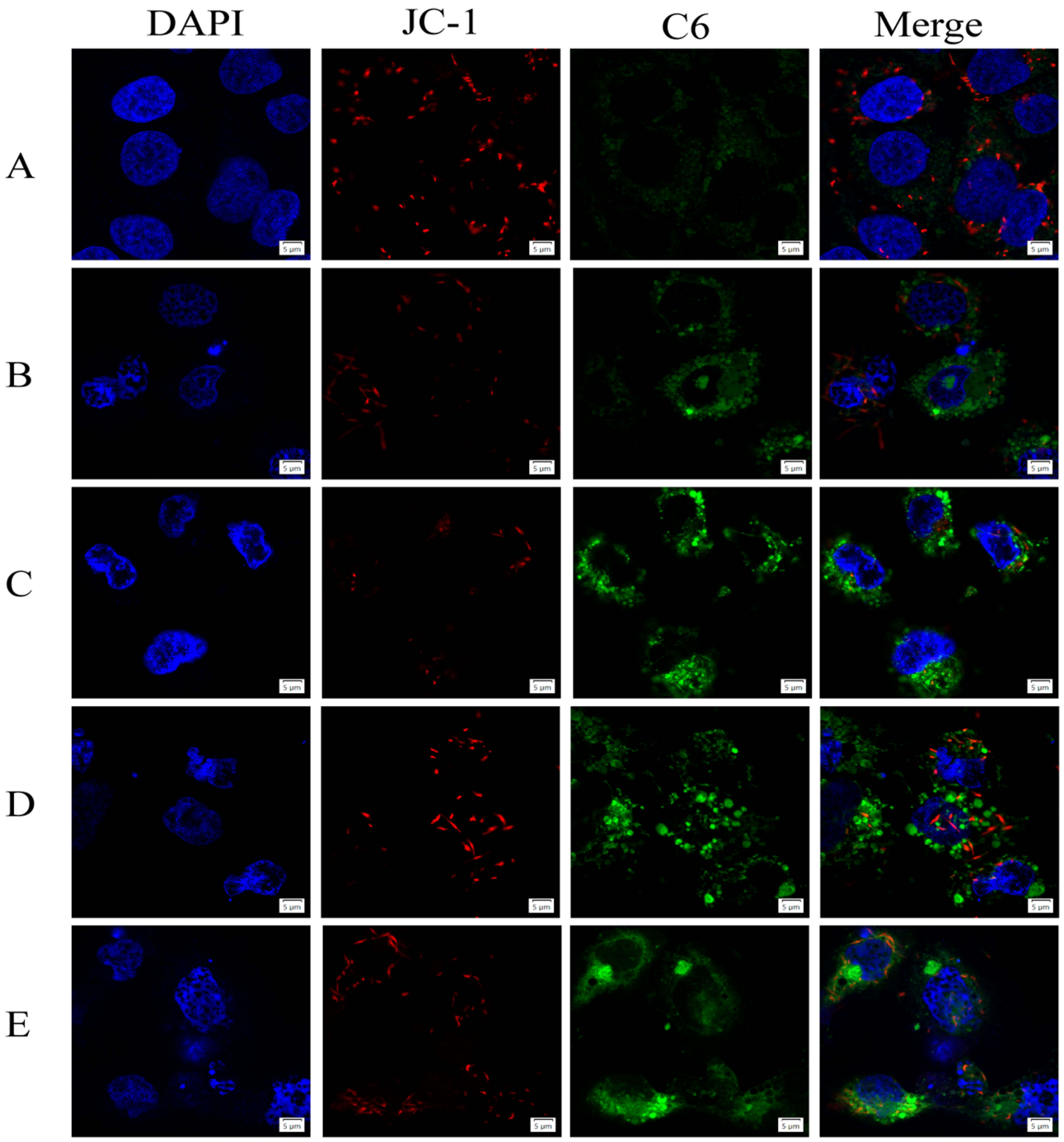

Figure 5 Uptake of liposomes modified with different ligands by Huh-7 cells.(**A**) Free C6; (**B**)C6- Lips; (**C**) FA-C6- Lips; (**D**) TPP-C6- Lips; (**E**) FA+TPP-C6- Lips.

by FA and TPP could be effectively delivered to the mitochondria and caused a decrease in mitochondrial membrane potential, while FA-TP-Lips and TP-Lips aggregated less in the mitochondria.

ROS Level Detection

The production of ROS mainly occurs in the mitochondria of cells, and mitochondrial damage is closely related to high levels of ROS. The results are illustrated in Figure 8. The ROS levels in TP solution, sorafenib, TP-Lips, FA-TP-Lips, TPP-TP-Lips and FA+TPP-TP-Lips groups were higher than that in blank group, and the ROS level in FA+TPP-TP-Lips group was the most significantly increased. The ROS level was basically consistent with the results of above

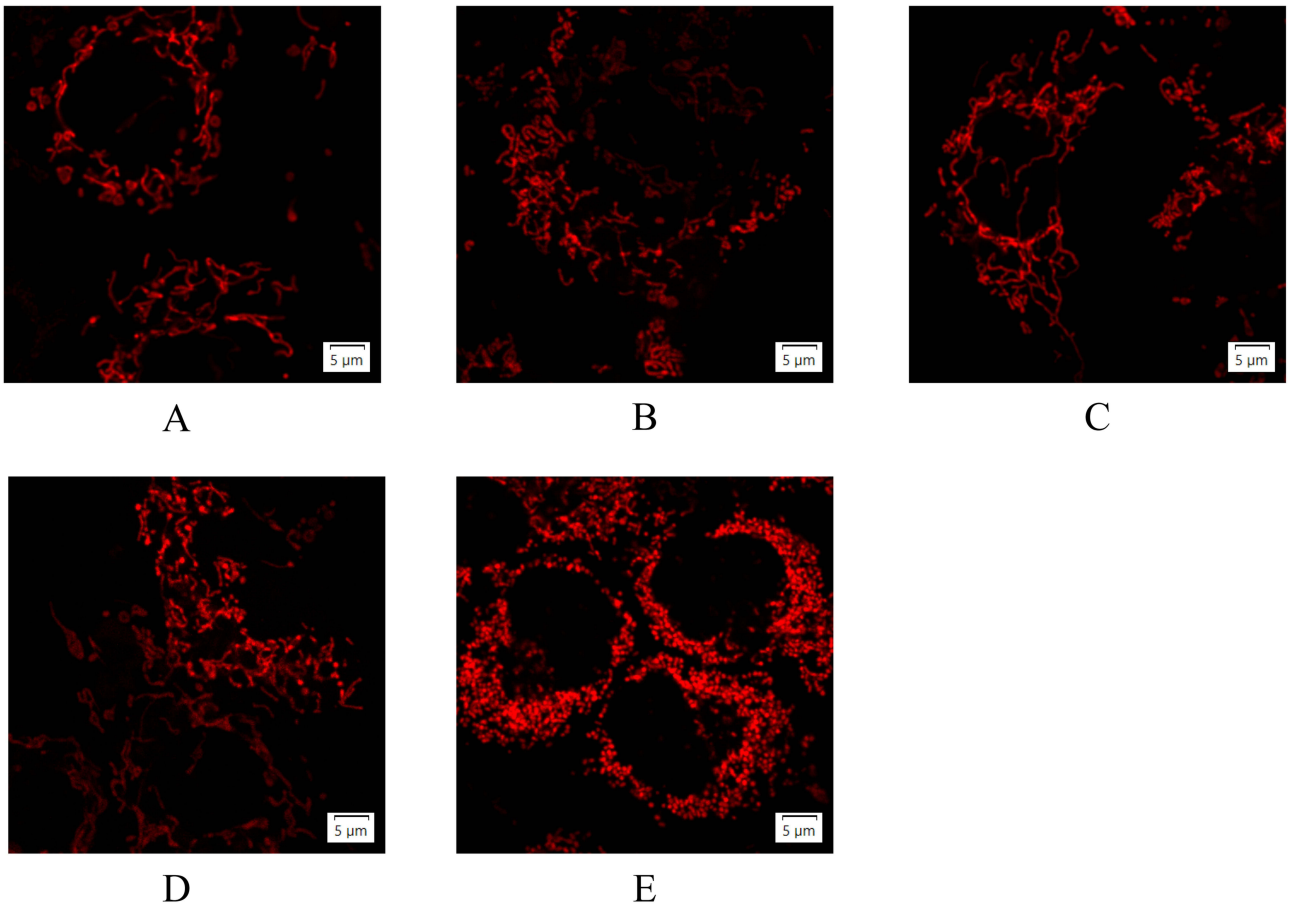

Figure 6 Mitochondrial morphology of Huh-7 cells after treatment with liposomes modified with different ligands (n=3). (**A**) Free TP; (**B**) TP-Lips; (**C**) FA-TP-Lips; (**D**) TPP-TP- Lips; (**E**) FA+TPP-TP-Lips.

mitochondrial membrane potential assay, confirming that FA+TPP-TP-Lips could increase the level of intracellular ROS, cause mitochondrial damage, thus decrease mitochondrial membrane potential.

Apoptosis Detection

Flow cytometry was used to evaluate the effects of FA+TPP-TP-Lips on the apoptosis of Huh-7 cells (Figure 9). Forward scatter (FSC) and side scatter (SSC) were used to distinguish the live cells from the dead cells and debris. After 48 h of treatment, many viable cell could be observed in the blank group, and the apoptosis rate was 3.16 ± 0.20%. The apoptosis rates in all treated groups were significantly higher than that in the blank group ($P < 0.01$). The apoptosis rates in TP-Lips, FA-TP-Lips, TPP-TP-Lips and FA+TPP-TP-Lips groups were significantly higher than that in the Free TP group (14.9± 3.60%) at the same concentration. Among these, FA+TPP-TP-Lips exhibited a stronger apoptosis-inducing ability on Huh-7 cells(43.26± 2.56%).

In vivo Liver Targeting Experiments/In vivo Distribution

To investigate the biodistribution of liposomes in vivo, FA-Cy5.5-Lips, TPP-Cy5.5-Lips, FA+TPP-Cy5.5-Lips, and Cy5.5-Lips were created by replacing TP with the Cy5.5 fluorescent dye. The in vivo fluorescence imager was used to observe and compare the distribution of liposomes at 16 and 24 h after injection. Significant fluorescence distribution of liposomes was observed in tumour tissues, especially the liposomes modified by FA and TPP, indicating that liposomes have active targeting ability in vivo (Figure 10A). Furthermore, by dissecting and performing ex vivo fluorescence imaging of the major organs and tumour tissues of mice 24 h after drug administration, the significant fluorescence was observed in tumour tissues of FA+TPP-Cy5.5-Lips group, and its fluorescence intensity was stronger than that of FA-

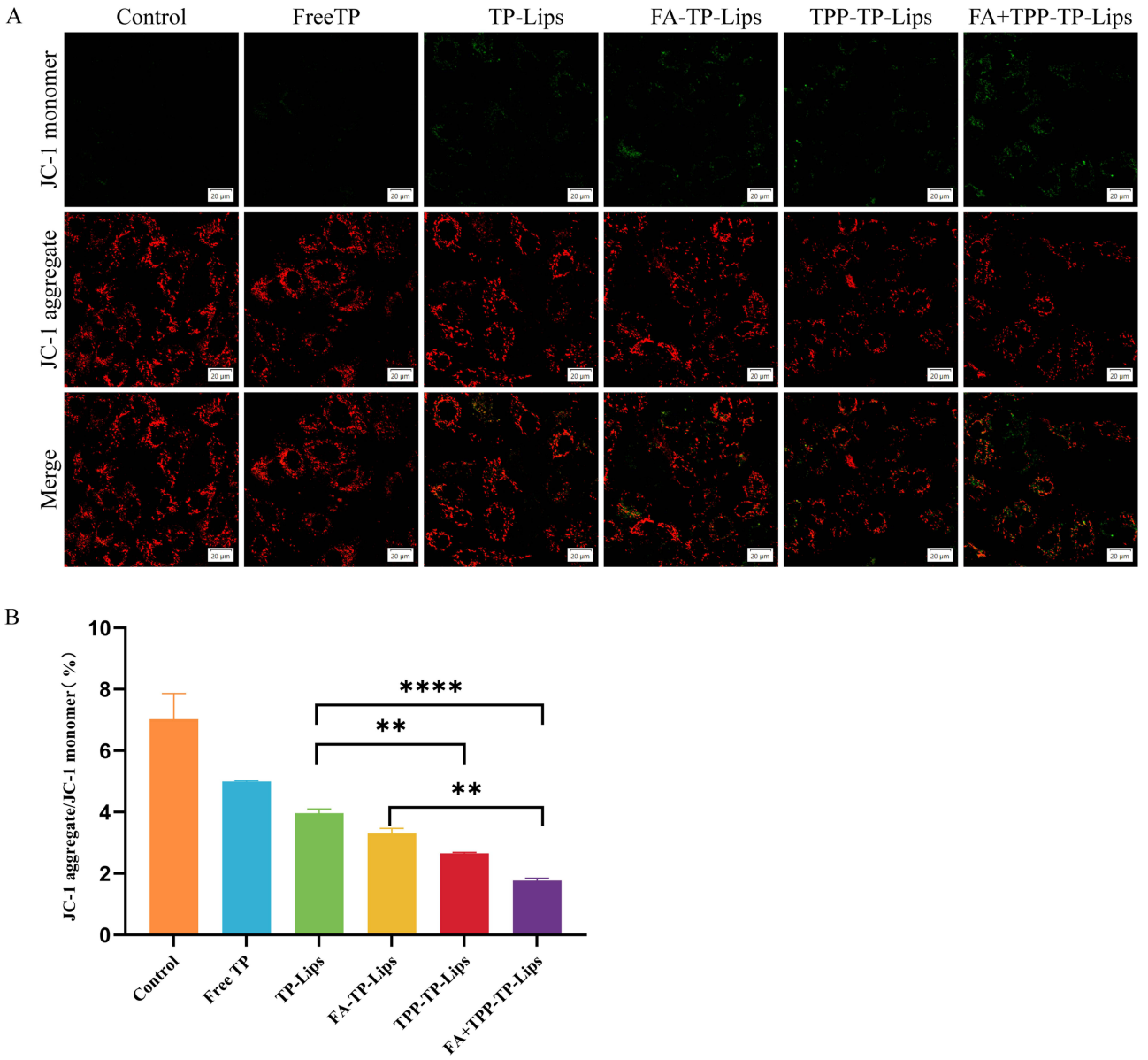

Figure 7 Effects of liposome intervention on mitochondrial membrane potential (n = 3). (**A**) Microscopic images of mitochondrial membrane potential; (**B**) Histogram of the fluorescence intensity ratio of JC-1 aggregate/JC-1 monomer.Data are expressed as the mean±SD (n=3). $^{**}p < 0.01$, $^{****}p < 0.0001$.

Cy5.5-Lips group and TPP-Cy5.5-Lips group, which was consistent with the result of in vivo distribution (Figure 10B). In conclusion, the mitochondria-targeting nanoliposomes constructed in this study can efficiently target liver tumour cells to deliver drugs, which will be beneficial to improve the therapeutic efficacy of TP and reduce non-specific side effects.

In vivo Antitumour Effects

The in vivo antitumour effects of liposomes were studied in the Huh-7 liver tumour model, as shown in Figure 11. The growth rate of tumour volume in each liposome group was significantly reduced compared with the TP solution group, and the liposome encapsulation exerted a good "increasing efficacy" effect (Figure 11B). Among them, FA+TPP-TP-Lips exhibited the best antitumour effect, with the smallest tumour mass (Figure 11C) and a tumour inhibition rate of 79.37%, while the tumour inhibition rates of the TP solution, TP-Lips, FA-TP-Lips and TPP-TP-Lips groups were 11.79%, 24.63%, 51.37%, and 42.32%, respectively. The tumour inhibitory effect of FA+TPP-TP-Lips was further confirmed by H&E staining (Figure 11D). Furthermore, the FA+TPP-TP-Lips group demonstrated the strongest inhibitory effect on

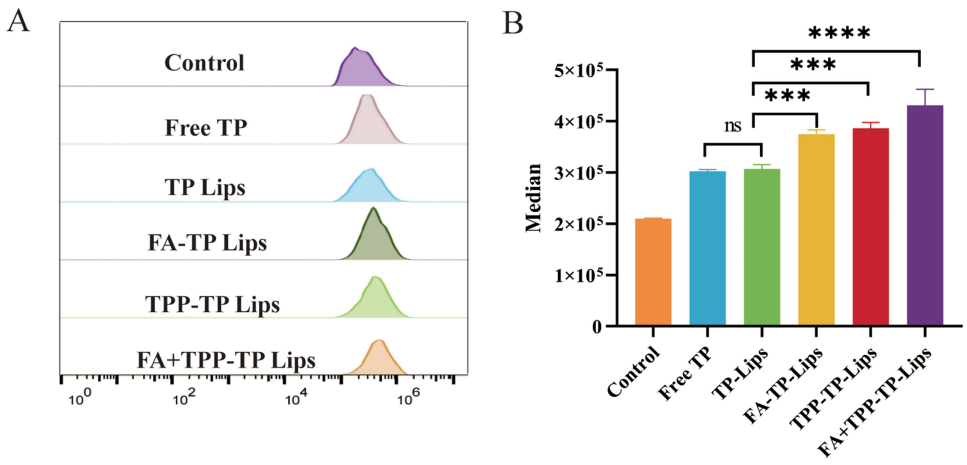

Figure 8 Effect of different liposomal interventions on ROS levels in Hun-7 cells (n = 3). (**A**) Quantification of ROS levels in Hun-7 cells using flow cytometry. (**B**) Statistical analysis of ROS levels. Data are expressed as the mean±SD (n=3). ns, not significant, ***$p < 0.001$, ****$p < 0.0001$.

cell proliferation compared with the other liposomes, with the lowest proliferation index of 23.4% in the PCNA assay and the highest apoptosis index of 13.4% in the TUNEL assay (Figure 11E and F).

Safety Evaluation

The in vivo toxicity of nano-formulations in the treatment of tumours is an important aspect to evaluate their practicability. Pathological analyses of the major organs of the nude mice were performed to evaluate the pathological changes of these organs at the end of the dosing cycle. The H&E staining results for each group demonstrated that the organs in the saline group exhibited intact and well-arranged cellular structures and clear staining of the nuclei (Figure 12A). Compared with the blank group, no pathological changes were observed in the heart, liver, spleen, lungs, and kidneys of nude mice in the FA+TPP-TP-Lips, FA-TP-Lips, TP-Lips and TP solution groups, indicating that there were no obvious injuries or lesions in the major organs of nude mice during drug administration. Analysis of Figure 12B demonstrates that compared with the saline group, the concentration of AST in other groups were significantly increased. However, there was no significant increase in ALT, BUN, or CREA levels, indicating that the drug-carrying liposome had some damage to liver function, but no significant damage to the kidneys. Moreover, no significant changes in body weight were observed in mice treated with the modified liposomes, indicating that they were well tolerated at the tested dose levels (Figure 12C).

Discussion

Hepatocellular carcinoma is characterized by significant heterogeneity, encompassing a variety of pathological subtypes and exhibiting a complex pathogenesis. The traditional treatment exhibits limited anti-cancer efficacy due to the toxicity and adverse side effects of drugs on normal tissues, as well as the development of drug resistance in tumor cells. Natural products such as paclitaxel have been used in the clinical treatment of cancer. Triptolide exhibits potent anti-cancer properties across a range of malignancies, including hepatocellular carcinoma, and is consequently regarded as a promising chemotherapeutic agent for the treatment of malignant tumors. Nevertheless, the limited water solubility and significant toxicity of TP impede its potential for clinical application.[34] To enhance the anti-cancer efficacy of TP while mitigating its toxic side effects, we developed FA+ TPP-TP-Lips. FA+ TPP-TP-Lips overcomes the problems of low solubility and toxicity of TP through its encapsulation effect and the property of actively targeting tumor tissue and intracellular mitochondria. In this study, FA+TPP-TP-Lips were prepared using the thin film dispersion technique. The optimal ratio of soybean lecithin to the drug was determined through preliminary experimentation. Based on the analysis of particle size, zeta potential, and encapsulation efficiency, the ratio was established to be 15:1. FA-PEG_{3400}-DSPE and TPP-PEG_{2000}-TK-DSPE are modified on the surface of the liposomes to avoid the mononuclear phagocytic system to ensure long-term blood circulation of liposomes. Due to the accelerated proliferation of tumor tissue compared to normal

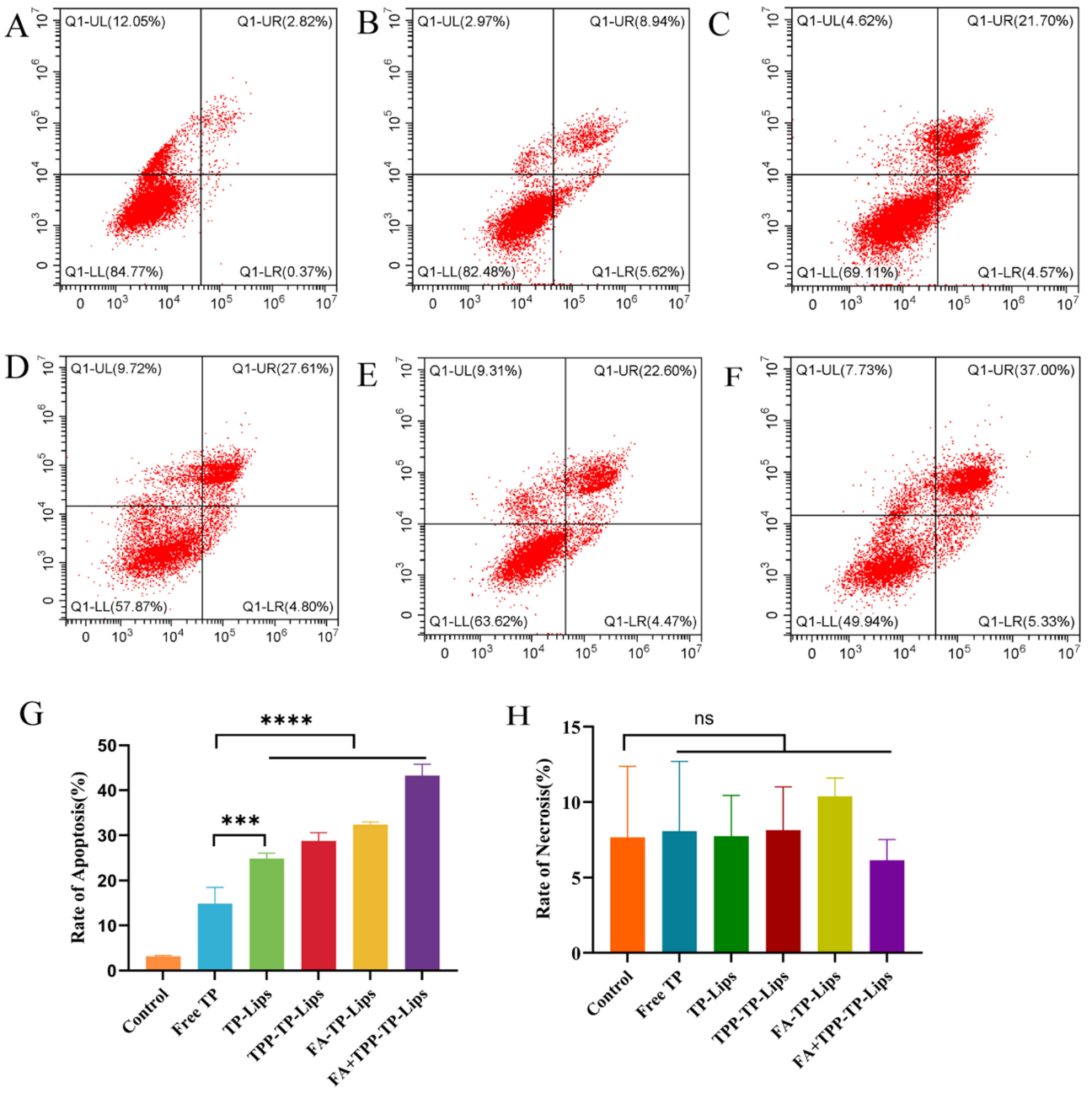

Figure 9 Effect of liposome treatment on apoptosis of Huh-7 cells (n = 3).(**A**) Control; (**B**) Free TP; (**C**) TP-Lips; (**D**) FA-TP-Lips; (**E**) TPP-TP-Lips; (**F**) FA+TPP-TP-Lips. (**G**) Quantitative data of apoptosis rate of Huh-7 cells. Data are expressed as the mean±SD (n=3). (**H**) Quantitative data of necrosis rate of Huh-7 cells. Data are expressed as the mean±SD (n=3). ns, not significant. ***p < 0.001, ****p < 0.0001.

tissue, the vascular walls at the tumor site exhibit a distinctively permeable structure. This characteristic facilitates the penetration of nano-sized liposomes through the vascular walls into the interstitial space of the tumor tissue. The particle size of liposomes is crucial for their effective penetration and accumulation within tumor tissues, which is facilitated by the enhanced permeability and retention (EPR) effect associated with tumor vascular leakage. The particle size of FA+TPP-TP-Lips was measured using dynamic light scattering, revealing an approximate size of 100 nm. Consequently, FA+TPP-TP-Lips are expected to exhibit favorable aggregation within tumor tissues, a phenomenon that has been corroborated through in vivo fluorescence imaging and fluorescence imaging of major organs and tumors.

Mitochondrial damage, as a central regulator of apoptosis, can alter the permeability of the mitochondrial membrane, resulting in the release of apoptotic factors such as cytochrome C, thereby further inducing apoptosis.[49]

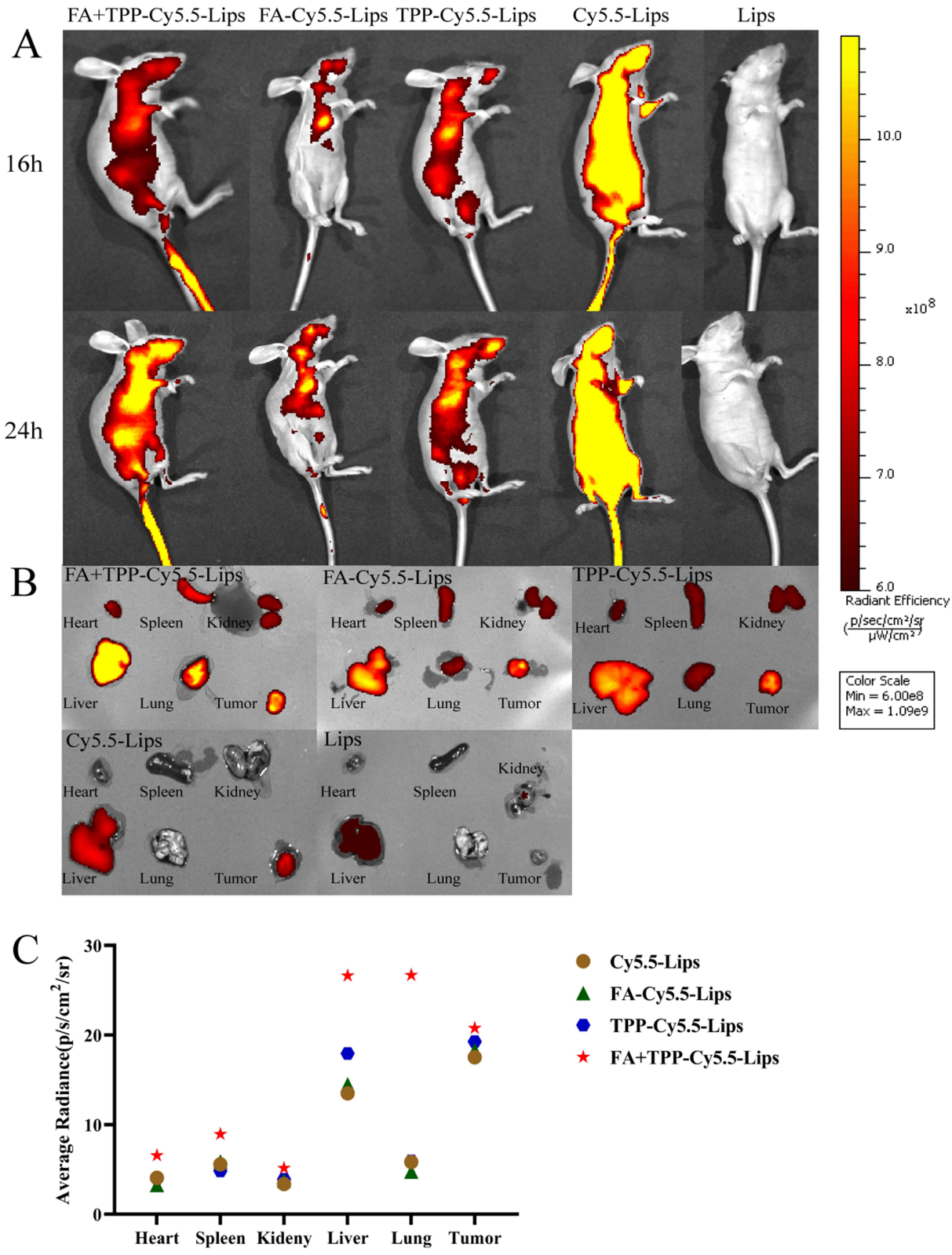

Figure 10 Fluorescence images of (**A**) in vivo and (**B**) in vitro hormonal mice after treatment with different therapeutic methods. (**C**) The quantitative data of average radiance (p/s/cm^2/sr) in each organ.

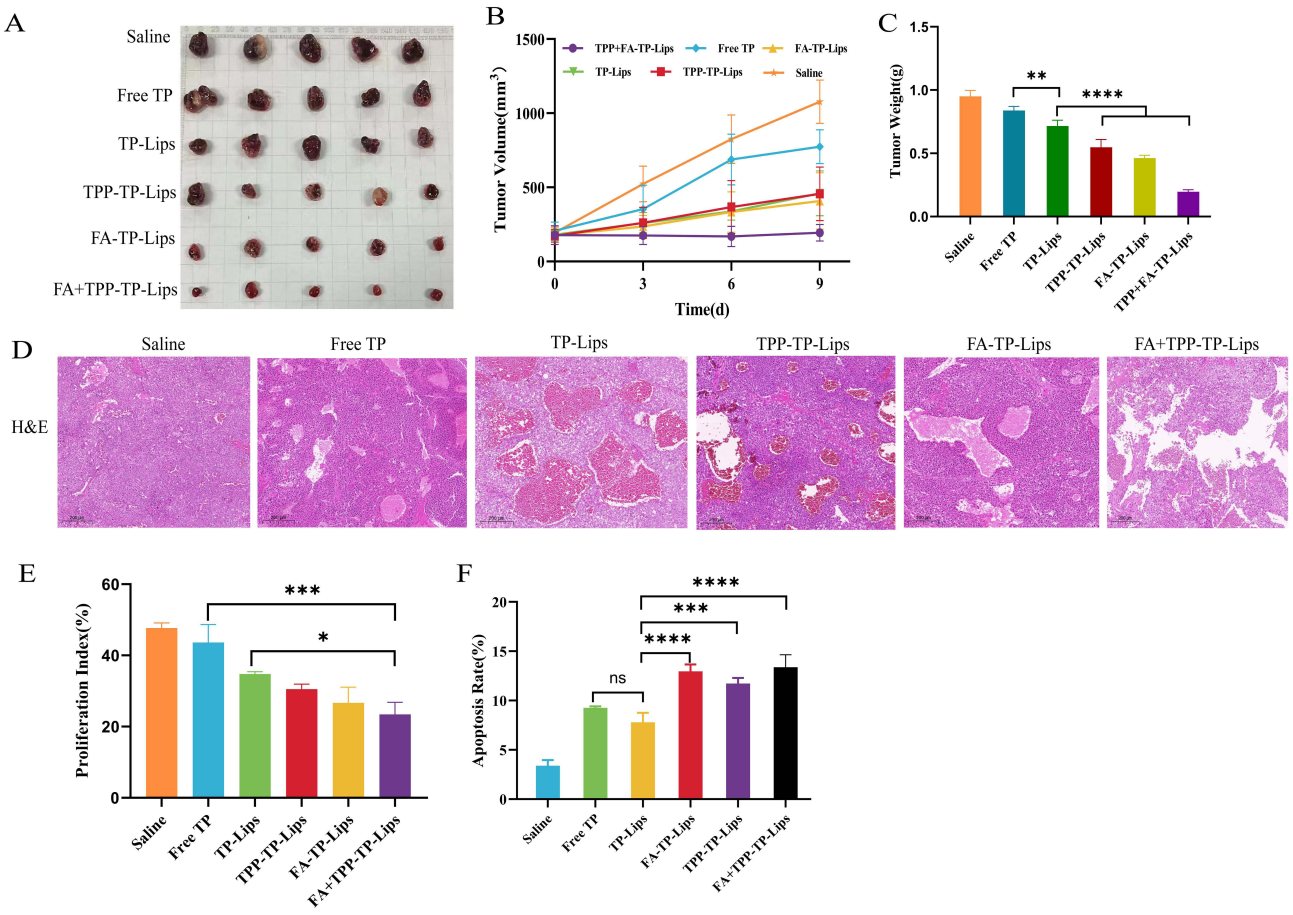

Figure 11 In vivo antitumour effects. (**A**) Tumors collected on day 12 (**B**) Tumor volume growth curve (**C**) Tumor weight. Data are expressed as the mean±SD (n=5). (**D**) H&E staining of tumor sections (**E**) Tumor proliferation index of BALB/C nude mice bearing tumor. Data are expressed as the mean±SD (n=3). (**F**) Apoptosis rate of tumor in BALB/C nude mice. Data are expressed as the mean±SD (n=3). *p < 0.05, **p < 0.01, ***p < 0.001, ****p < 0.0001, ns, not significant.

Triphenylphosphonium (TPP) lipophilic cations exhibit properties that enable them to specifically target mitochondria. The fat-solubility of TPP facilitates its permeation through cellular and mitochondrial membranes. On the other hand, due to its positive charge, TPP preferentially accumulates in the mitochondria of tumor cells, which exhibit a higher transmembrane potential compared to normal cells, thereby allowing lipophilic cations to selectively concentrate within cancer cell mitochondria. TPP is characterized by a positive charge, whereas the tumor cell membrane exhibits a negative charge ranging from −30 to −60 mV, and the mitochondrial inner membrane possesses a negative charge between −150 and −180 mV. The electrostatic attraction between the positively charged TPP cations and the negatively charged membranes significantly enhances the accumulation of TPP within mitochondria, by a factor of 100 to 500. This accumulation effectively overcomes the barrier posed by the high viscosity of the intracellular fluid, facilitating the transmembrane transport of liposomes. Consequently, TPP mediates the targeted delivery of anticancer drugs into mitochondria, thereby augmenting their antitumor efficacy. To facilitate efficient mitochondrial transport, liposomes must possess a substantial positive charge. The zeta potential measurements for TPP-TP-Lips and FA+TPP-TP-Lips were 2.17±0.23 mV and 1.2±0.08 mV, respectively, in contrast to the −2.68±0.83 mV observed for TP-Lips. Following TPP modification, these liposomes demonstrated a marked ability to accumulate within mitochondria, as corroborated by mitochondrial targeting studies.

The mitochondrial membrane potential is intricately associated with the process of cellular apoptosis. The depolarization of mitochondrial membrane potential represents one of the initial events in the apoptotic cascade. Once the mitochondrial membrane potential is compromised, the progression to cellular apoptosis becomes irreversible. Consequently, alterations in mitochondrial membrane potential might serve as an indirect indicator of a drug's capacity to target mitochondria. The

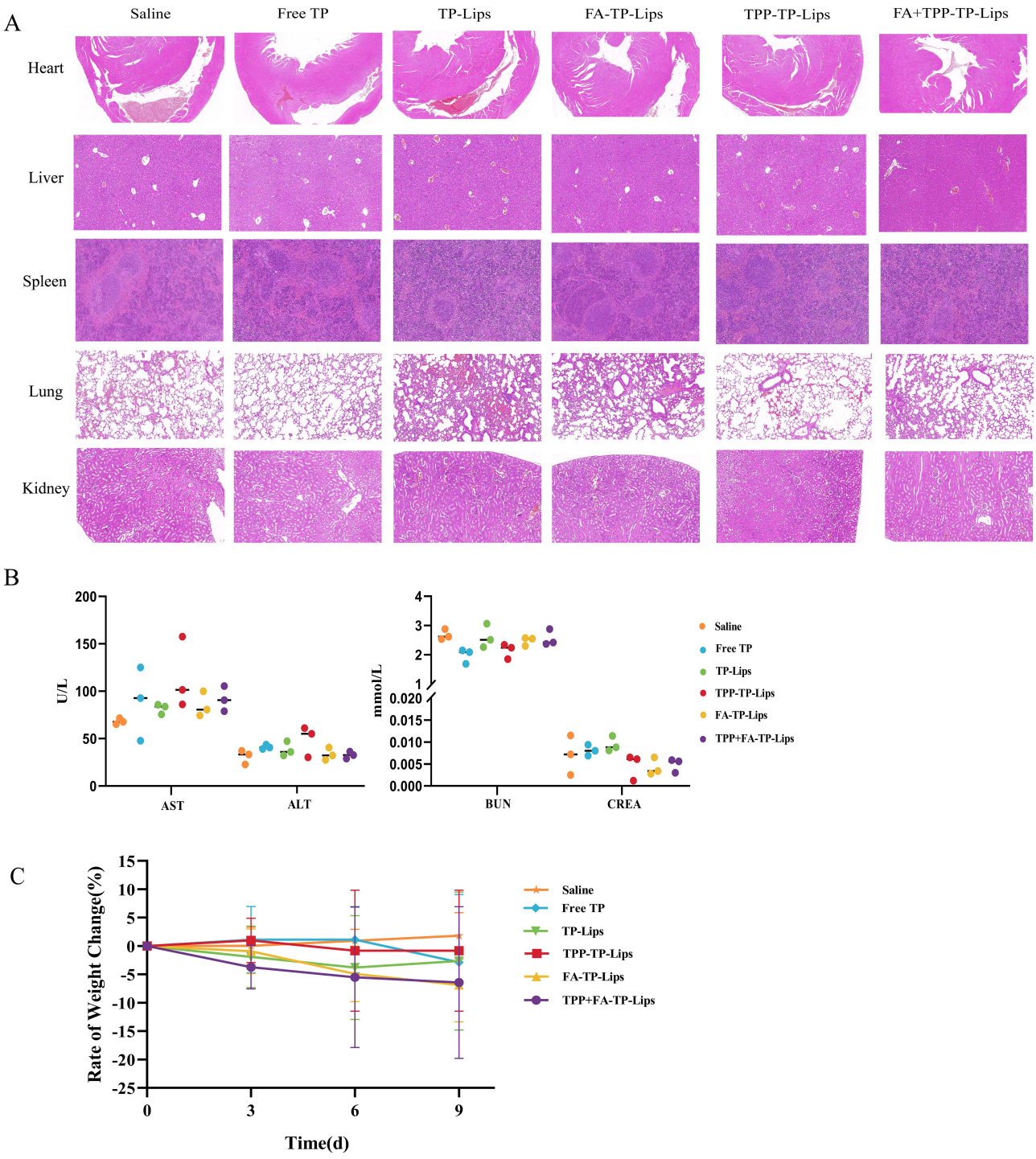

Figure 12 Safety evaluation of liposomes. (**A**) H&E staining of the organs of Homer BALB/C nude mice (n=3). (**B**) Results of biochemical indexes of the liver and kidney in each group of Homer BALB/C nude mice (n= 3). (**C**) Change rate of body weight in BALB/C nude mice during the administration cycle (n=5).

mitochondrial membrane potential was detected by JC-1 staining to further determine FA+ TPP-TP-Lips' mitochondrial targeting effect. The findings from the CCK-8 and JC-1 staining assays, along with apoptosis experiments, demonstrated that the modification of liposome surfaces with FA-PEG_{3400}-DSPE significantly enhanced cellular uptake of TP. Furthermore, the incorporation of the mitochondrial targeting moiety TPP facilitated increased accumulation of TP within mitochondria, thereby augmenting its therapeutic efficacy. FA+TPP-TP-Lips resulted in an increase in mitochondrial accumulation, which enhanced the cytotoxic effects through significant depolarization of the mitochondrial membrane potential. This targeting of

mitochondria facilitated the regulation of mitochondrial function, thereby initiating the apoptotic pathway and leading to extensive apoptosis in Huh-7 cells, with the most pronounced apoptotic effect observed.

Regarding tumor inhibition, the FA+TPP-TP-Lips group demonstrated a superior anti-tumor effect compared to the other groups. After nine days of treatment, this group exhibited the smallest tumor volume, which was significantly reduced relative to the other groups. Immunohistological examination of tumor sections revealed alterations in the morphology of tumor cells within the FA+TPP-TP-Lips treatment group. Notably, there was a reduction in tumor cell density, disappearance of some nuclei, and an expansion of the central space within the tumor tissue. Furthermore, the proliferation index, assessed via PCNA staining, was observed to be the lowest, while the apoptosis index, evaluated using TUNEL assay, was the highest among the groups studied. The findings indicated that the FA+TPP-TP-Lips treatment group had significant anti-tumor effects, primarily attributed to enhanced anti-proliferative and apoptosis-inducing properties. Toxicity continues to be a critical consideration in assessing the potential applications of pharmaceutical formulations and represents the primary impediment to the utilization of TP. On the final day of treatment, the FA+TPP-TP-Lips group did not exhibit a significant reduction in body weight compared to the saline group. This observation suggested that FA+TPP-TP-Lips could effectively mitigate systemic toxicity. Histological examination of hematoxylin and eosin (H&E) stained sections of major organs revealed that FA+ TPP-TP-Lips administration did not induce significant damage or lesions. These findings indicate that FA+ TPP-TP-Lips exhibit potent tumor suppressor activity while maintaining low systemic toxicity.

Conclusions

In this study, a nano-formulation (FA+TPP-TP-Lips) for targeting the mitochondrial of liver tumour cells was prepared by the thin film dispersion method, which could induce massive apoptosis of hepatocellular carcinoma cells by increasing ROS levels in hepatocellular carcinoma cells and decreasing the mitochondrial membrane potential. The nano-formulation had good physicochemical properties, which could aggregate around the mitochondria of the tumour cells, release TP to exert antitumour effects by FA-mediated liver tumour targeting and TPP-mediated mitochondrial targeting. The results of cytotoxicity assay revealed that the inhibition rate of FA+TPP-TP-Lips on Huh-7 cells was up to 98%, and the laser confocal microscopy results revealed significant mitochondrial damage. In vivo experiments revealed that FA+TPP-TP-Lips could be administered intravenously to achieve the highly targeting to tumour and mitochondrial with negligible adverse effects on normal tissues. In conclusion, the FA+TPP-TP-Lips constructed in this study exhibited good targeting to the mitochondrial of liver tumours, which could improve the aggregation of drugs in tumour tissues and organelles, achieve the purpose of increasing efficiency and reducing toxicity and provide a feasible solution for the treatment of hepatocellular carcinoma with TP.

Ethics Approval and Consent to Participate

In this study, all methods were carried out in accordance with relevant guidelines and regulations.The animal experiments conducted in this study were approved by the Animal Management Committee of Hunan University of Chinese Medicine.All procedures on animals were in compliance with the animal protection agreements and regulations.

Author Contributions

All authors made a significant contribution to the work reported, whether that is in the conception, study design, execution, acquisition of data, analysis and interpretation, or in all these areas; took part in drafting, revising or critically reviewing the article; gave final approval of the version to be published; have agreed on the journal to which the article has been submitted; and agree to be accountable for all aspects of the work.

Funding

This study was supported by Natural Science Foundation of Hunan Province (No. 2022JJ40320), the Excellent Youth Project of Hunan Provincial Department of Education (No. 23B0362), the Key Projects of Hunan University of Chinese Medicine (No.Z2023XJZD05), the General Subjects of Hunan Provincial Administration of Traditional Chinese Medicine(No. B2024015), the Key Discipline Project on Chinese Pharmacology of Hunan University of Chinese Medicine [202302].

Disclosure

The authors declare that they have no known competing financial interests or personal relationships that could have appeared to influence the work reported in this paper.

References

1. Zheng Y, Niu X, Xue W, et al. The Role of Alternative Splicing Factors hnRNP G and Fox-2 in the Progression and Prognosis of Esophageal Cancer. *Dis Markers*. 2022;2022:3043737. doi:10.1155/2022/3043737
2. Ueshima E, Nishiofuku H, Takaki H, et al. Hepatic Artery Embolization Induces the Local Overexpression of Transforming Growth Factor β1 in a Rat Hepatoma Model. *Liver Cancer*. 2020;9(1):63–72. doi:10.1159/000502774
3. Yu G, Ali Z, Sajjad Khan A, et al. Preparation, Pharmacokinetics, and Antitumor Potential of Miltefosine-Loaded Nanostructured Lipid Carriers. *Int J Nanomed*. 2021;16:3255–3273. doi:10.2147/IJN.S299443
4. Chen ZW, Hu J-F, Wang Z-W, et al. Circular RNA circ-MTHFD1L induces HR repair to promote gemcitabine resistance via the miR-615-3p/RPN6 axis in pancreatic ductal adenocarcinoma. *J Exp Clin Cancer Res*. 2022;41(1):153. doi:10.1186/s13046-022-02343-z
5. Fialho MFP, Brum ES, Becker G, et al. Kinin B(2) and B(1) Receptors Activation Sensitize the TRPA1 Channel Contributing to Anastrozole-Induced Pain Symptoms. *Pharmaceutics*. 2023;15(4):1136. doi:10.3390/pharmaceutics15041136
6. Liu Y, Liu L. Changes in the Epidemiology of Hepatocellular Carcinoma in Asia. *Cancers*. 2022;14(18).
7. Kido T. Potential dual functional roles of the Y-linked RBMY in hepatocarcinogenesis. *Cancer Sci*. 2020;111(8):2987–2999. doi:10.1111/cas.14506
8. Zhao J. P7TP3 inhibits tumor development, migration, invasion and adhesion of liver cancer through the Wnt/β-catenin signaling pathway. *Cancer Sci*. 2020;111(3):994–1007. doi:10.1111/cas.14243
9. Llovet Josep M, Montal R, Sia D, et al. Molecular therapies and precision medicine for hepatocellular carcinoma.[J].Nature reviews. *Clin Oncol*. 2018;15(8):599–616. doi:10.1038/s41571-018-0073-4
10. Yang Y, et al. Compound kushen injection relieves tumor-associated macrophage-mediated immunosuppression through TNFR1 and sensitizes hepatocellular carcinoma to sorafenib. *J ImmunoTher Cancer*. 2020;1:e000317.
11. Sung H. Global Cancer Statistics 2020: GLOBOCAN Estimates of Incidence and Mortality Worldwide for 36 Cancers in 185 Countries[J]. *Ca a Cancer J Clinicians*. 2021;3:209–249.
12. Hao Y, Li X. Deacetylated-poly-N-acetylglucosamine-folic Acid as a Nanocarrier for Delivering miR-196a Inhibitor to Anticancer Activity. *Balkan Med J*. 2022;39(1):55–65. doi:10.4274/balkanmedj.galenos.2021.2021-8-62
13. Yang S, Pang L, Dai W, et al. Role of Forkhead Box O Proteins in Hepatocellular Carcinoma Biology and Progression (Review). *Front Oncol*. 2021;11:667730. doi:10.3389/fonc.2021.667730
14. Ding J, Jin Y, Zhu F, et al. Facile Synthesis of NaYF4: Yb Up-Conversion Nanoparticles Modified with Photosensitizer and Targeting Antibody for In Vitro Photodynamic Therapy of Hepatocellular Carcinoma. *J Healthc Eng*. 2022;2022:4470510. doi:10.1155/2022/4470510
15. Miao YQ, Chen M-S, Zhou X, et al. Chitosan oligosaccharide modified liposomes enhance lung cancer delivery of paclitaxel. *Acta Pharmacol Sin*. 2021;42(10):1714–1722. doi:10.1038/s41401-020-00594-0
16. Gu Y, Du Y, Jiang L, et al. αvβ3 integrin-specific exosomes engineered with cyclopeptide for targeted delivery of triptolide against malignant melanoma. *J Nanobiotechnology*. 2022;20(1):384. doi:10.1186/s12951-022-01597-1
17. Sun R, Dai J, Ling M, et al. Delivery of triptolide: a combination of traditional Chinese medicine and nanomedicine. *J Nanobiotechnology*. 2022;20(1):194. doi:10.1186/s12951-022-01389-7
18. Yuan F, Sun M, Liu Z, et al. Macropinocytic dextran facilitates KRAS-targeted delivery while reducing drug-induced tumor immunity depletion in pancreatic cancer. *Theranostics*. 2022;12(3):1061–1073. doi:10.7150/thno.65299
19. Que H, Hong W, Lan T, et al. Tripterin liposome relieves severe acute respiratory syndrome as a potent COVID-19 treatment. *Signal Transduct Target Ther*. 2022;7(1):399. doi:10.1038/s41392-022-01283-6
20. Wu H, Rao Q, Ma G-C, et al. Effect of Triptolide on Dextran Sodium Sulfate-Induced Ulcerative Colitis and Gut Microbiota in Mice. *Front Pharmacol*. 2019;10:1652. doi:10.3389/fphar.2019.01652
21. Li H, Li L, Mei H, et al. Antitumor properties of triptolide: phenotype regulation of macrophage differentiation. *Cancer Biol Ther*. 2020;21(2):178–188. doi:10.1080/15384047.2019.1679555
22. Zheng Y, Kong F, Liu S, et al. Membrane protein-chimeric liposome-mediated delivery of triptolide for targeted hepatocellular carcinoma therapy. *Drug Deliv*. 2021;28(1):2033–2043. doi:10.1080/10717544.2021.1983072
23. Deng QD, Lei X-P, Zhong Y-H, et al. Triptolide suppresses the growth and metastasis of non-small cell lung cancer by inhibiting β-catenin-mediated epithelial-mesenchymal transition. *Acta Pharmacol Sin*. 2021;42(9):1486–1497. doi:10.1038/s41401-021-00657-w
24. Zeng H, Zhu X, Tian Q, et al. In vivo antitumor effects of carboxymethyl chitosan-conjugated triptolide after oral administration. *Drug Deliv*. 2020;27(1):848–854. doi:10.1080/10717544.2020.1770370
25. Wang X, Zeng H, Zhu X, et al. TP-CSO: a Triptolide Prodrug for Pancreatic Cancer Treatment. *Molecules*. 2022;27(12).
26. Liu XY, Pei W-J, Wu Y-Z, et al. Transdermal delivery of triptolide-phospholipid complex to treat rheumatoid arthritis. *Drug Deliv*. 2021;28(1):2127–2136. doi:10.1080/10717544.2021.1986603
27. Zhao X, Tang X, Yan Q, et al. Triptolide ameliorates lupus via the induction of miR-125a-5p mediating Treg upregulation. *Int Immunopharmacol*. 2019;71:14–21.
28. Wang N, Min X, Ma N, et al. The Negative Impact of Triptolide on the Immune Function of Human Natural Killer Cells. *Pharmaceuticals (Basel)*. 2023;16(3). doi:10.3390/ph16030458
29. Viegas JSR, Praça FG, Kravicz M, et al. Therapeutic applications and delivery systems for triptolide. *Drug Deliv Transl Res*. 2020;10(6):1584–1600. doi:10.1007/s13346-020-00827-z
30. Zhu D, Zhang Q, Chen Y, et al. *Mechanochemical preparation of triptolide-loaded self-micelle solid dispersion with enhanced oral bioavailability and improved anti-tumor activity*. *Drug Deliv*. 2022;29(1):1398–1408. doi:10.1080/10717544.2022.2069879
31. Li M, Luo Q, Chen X, et al. Screening of major hepatotoxic components of Tripterygium wilfordii based on hepatotoxic injury patterns. *BMC Complement Med Ther*. 2023;23(1):9. doi:10.1186/s12906-023-03836-w

32. Liu X, Chen C, Han D, et al. SLC7A11/GPX4 Inactivation-Mediated Ferroptosis Contributes to the Pathogenesis of Triptolide-Induced Cardiotoxicity. *Oxid Med Cell Longev*. 2022;2022:3192607. doi:10.1155/2022/3192607
33. Jiang L, Gu Y, Du Y, et al. Engineering Exosomes Endowed with Targeted Delivery of Triptolide for Malignant Melanoma Therapy. *ACS Appl Mater Interfaces*. 2021;13(36):42411–42428. doi:10.1021/acsami.1c10325
34. Li L, He D, Guo Q, et al. Exosome-liposome hybrid nanoparticle codelivery of TP and miR497 conspicuously overcomes chemoresistant ovarian cancer. *J Nanobiotechnology*. 2022;20(1):50. doi:10.1186/s12951-022-01264-5
35. Cheng D, Wen Z, Chen H, et al. Hepatocyte-targeting and tumor microenvironment-responsive liposomes for enhanced anti-hepatocarcinoma efficacy. *Drug Deliv*. 2022;29(1):2995–3008. doi:10.1080/10717544.2022.2122635
36. Bo Y, Wang H. Materials-based vaccines for infectious diseases. *Wiley Interdiscip Rev Nanomed Nanobiotechnol*. 2022;14(5):e1824. doi:10.1002/wnan.1824
37. Zhang X, Zhao Q, Cao M, et al. Folate Receptor 4-Expressing T cell Is Associated with Disease-Free Survival in Patients with Esophageal Squamous Cell Carcinoma. *Dis Markers*. 2022;2022:4351949. doi:10.1155/2022/4351949
38. Clement S, Chen W, Deng W, et al. X-ray radiation-induced and targeted photodynamic therapy with folic acid-conjugated biodegradable nanoconstructs. *Int J Nanomed*. 2018;13:3553–3570. doi:10.2147/IJN.S164967
39. Wang R, Li N, Zhang T, et al. Tumor microenvironment-responsive micelles assembled from a prodrug of mitoxantrone and 1-methyl tryptophan for enhanced chemo-immunotherapy. *Drug Deliv*. 2023;30(1):2182254. doi:10.1080/10717544.2023.2182254
40. Parvathaneni V, Shukla SK, Gupta V. Development and Characterization of Folic Acid-Conjugated Amodiaquine-Loaded Nanoparticles-Efficacy in Cancer Treatment. *Pharmaceutics*. 2023;15(3):1001. doi:10.3390/pharmaceutics15031001
41. Grigoletto A, Martinez G, Gabbia D, et al. Folic Acid-Targeted Paclitaxel-Polymer Conjugates Exert Selective Cytotoxicity and Modulate Invasiveness of Colon Cancer Cells. *Pharmaceutics*. 2021;13(7). doi:10.3390/pharmaceutics13070929
42. Li M, Bian X, Chen X, et al. Multifunctional liposome for photoacoustic/ultrasound imaging-guided chemo/photothermal retinoblastoma therapy. *Drug Deliv*. 2022;29(1):519–533. doi:10.1080/10717544.2022.2032876
43. Kwon SM, Lee YK, Min S, et al. Mitoribosome Defect in Hepatocellular Carcinoma Promotes an Aggressive Phenotype with Suppressed Immune Reaction. *iScience*. 2020;23(6):101247.
44. Shen L, Zhan X, Angeloni C. Mitochondrial Dysfunction Pathway Alterations Offer Potential Biomarkers and Therapeutic Targets for Ovarian Cancer. *Oxid Med Cell Longev*. 2022;2022:5634724. doi:10.1155/2022/5634724
45. Zhang S, Zheng F, Liu Ket al. Mitochondria-Targeting Polymer Micelles in Stepwise Response Releasing Gemcitabine and Destroying the Mitochondria and Nucleus for Combined Antitumor Chemotherapy. *Int J Mol Sci*. 2022;23(20).
46. Huang Q, Yang Y, Zhao T, et al. Passively-targeted mitochondrial tungsten-based nanodots for efficient acute kidney injury treatment. *Bioact Mater*. 2023;21:381–393. doi:10.1016/j.bioactmat.2022.08.022
47. Lee JS, Oh H, Kim S, et al. A Novel Chitosan Nanosponge as a Vehicle for Transepidermal Drug Delivery. *Pharmaceutics*. 2021;13(9). doi:10.3390/pharmaceutics13091329
48. Li W, Chen Y, He K, et al. The Apoptosis of Liver Cancer Cells Promoted by Curcumin/TPP-CZL Nanomicelles With Mitochondrial Targeting Function. *Front Bioeng Biotechnol*. 2022;10:804513. doi:10.3389/fbioe.2022.804513
49. Xu S, Cheng X, Wu L, et al. Capsaicin induces mitochondrial dysfunction and apoptosis in anaplastic thyroid carcinoma cells via TRPV1-mediated mitochondrial calcium overload. *Cell Signal*. 2020;75:109733. doi:10.1016/j.cellsig.2020.109733